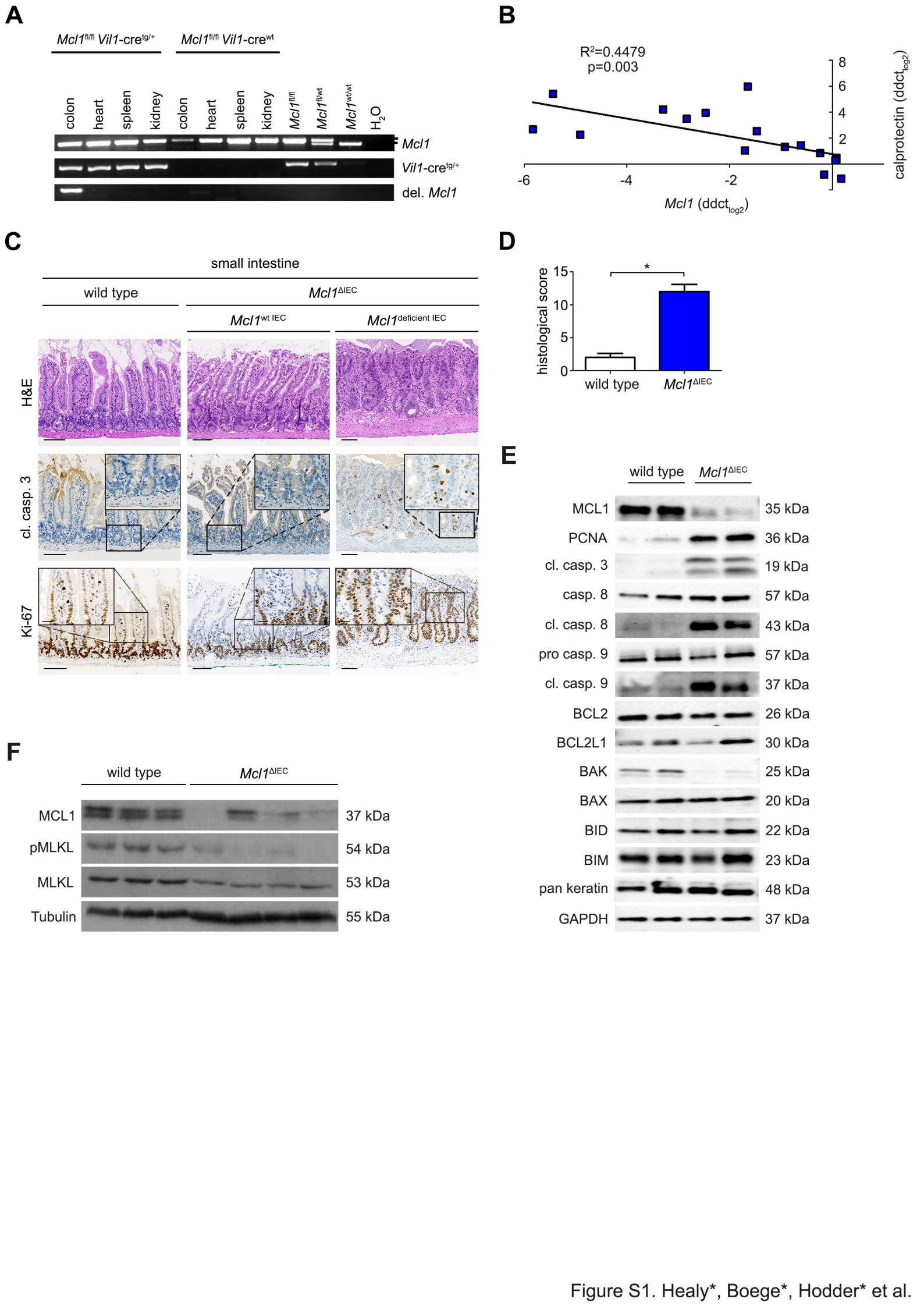

Figure S1. Healy*, Boege*, Hodder* et al.

Figure S1: Characterisation of *Mcl1*$^{\Delta IEC}$ mice. (*A*) Tissue specific PCR illustrating *Mcl1* deletion is specific to the intestine of *Mcl1*$^{fl/fl}$ *Vil1*-cre$^{tg/wt}$ (M*cl1*$^{\Delta IEC}$) mice and not *Mcl1*$^{fl/fl}$ *Vil1*-cre$^{wt/wt}$ (wild type) mice. (*B*) Real time PCR from whole colon tissue homogenates demonstrates that levels of calprotectin were inversely correlated to levels of *Mcl1* expression within 2-month-old *Mcl1*$^{\Delta IEC}$ mice (n=15). (*C*) Representative images from the small intestine of 2-month-old wild type control mice compared with *Mcl1*$^{\Delta IEC}$ littermate mice showing impaired intestinal architecture (H&E), increased IEC apoptosis (cl. casp. 3), and hyperproliferation (Ki-67) (scale bars: 100μm, 25μm for inserts). (*D*) Blinded histological scoring showing increased histological score in the small intestine of 2-month-old *Mcl1*$^{\Delta IEC}$ mice compared with wild type control mice (n=5). (*E*) Representative images of western blot analysis from IEC isolated from 2-month-old wild type and *Mcl1*$^{\Delta IEC}$ mice and analysed for markers of proliferation, apoptosis, as well as other BCL2 family members. (*F*) Representative images from western blot analysis showing no evidence of increased expression of the necroptosis markers MLKL or pMLKL in IEC isolated from 2-month-old *Mcl1*$^{\Delta IEC}$ mice suggesting that IEC death observed in *Mcl1*$^{\Delta IEC}$ mice is mediated through apoptosis rather than necroptosis. Tubulin was used as a loading control. Data presented as either bar charts or scatter plot graph show mean values ± s.e.m. Statistical analysis was conducted by Mann-Whitney test (*D*) where * $p \leq 0.05$.

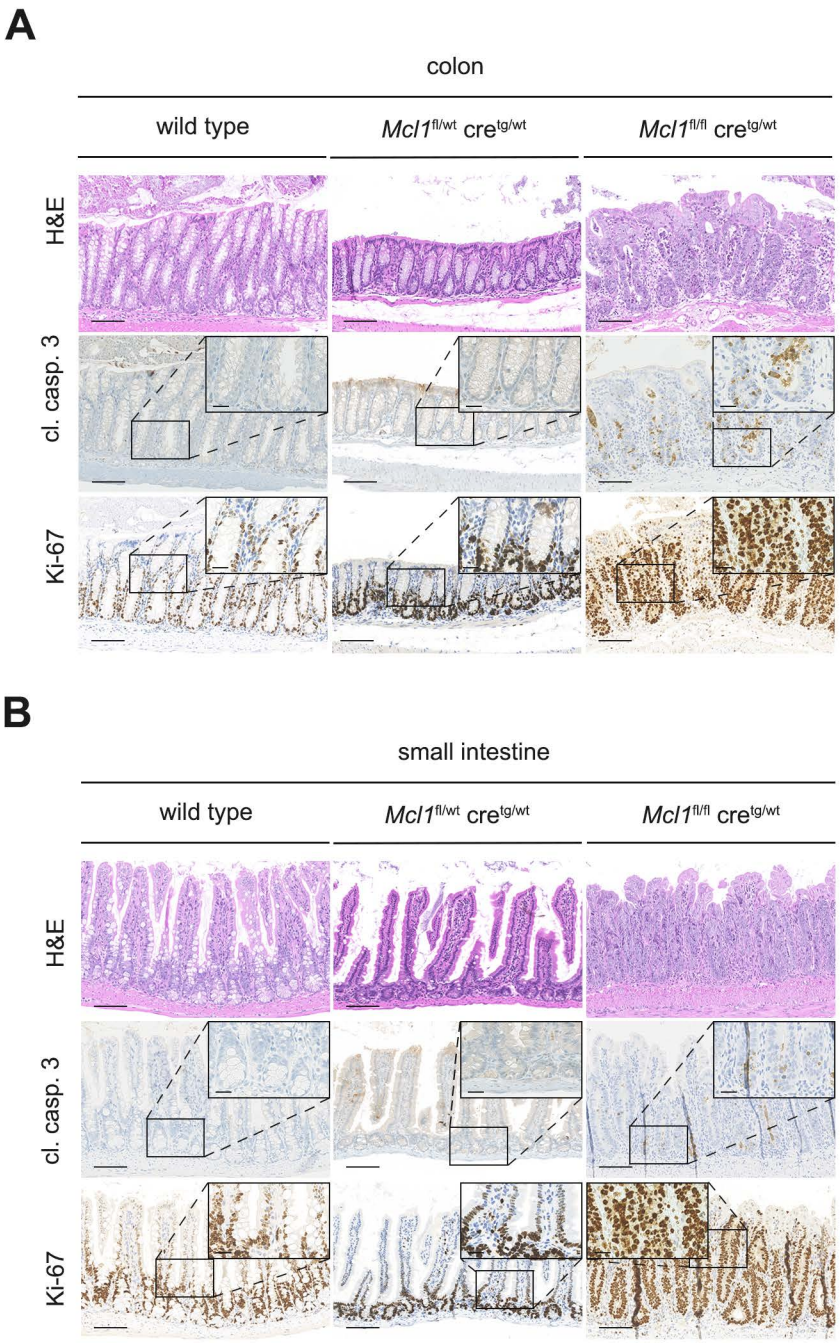

Figure S2. Healy*, Boege*, Hodder* et al.

Figure S2: *Mcl1*$^{fl/wt}$ cre$^{tg/wt}$ mice morphologically resemble wild type control mice. (A) Representative images from the colon of 2-month-old *Mcl1*$^{fl/wt}$ cre$^{tg/wt}$ control mice compared with wild type control and *Mcl1*$^{\Delta IEC}$ (*Mcl1*$^{fl/fl}$ cre$^{tg/wt}$) littermates showing normal intestinal architecture (H&E), no basal IEC apoptosis (cl. casp. 3), and normal levels of proliferation (Ki-67) (scale bars: 100μm, 25μm for inserts). (B) Representative images from the small intestine of 2-month-old *Mcl1*$^{fl/wt}$ cre$^{tg/wt}$ control mice compared with wild type control and *Mcl1*$^{\Delta IEC}$ (*Mcl1*$^{fl/fl}$ cre$^{tg/wt}$) littermates showing normal intestinal architecture (H&E), no basal IEC apoptosis (cl. casp. 3), and normal levels of proliferation (Ki-67) (scale bars: 100μm, 25μm for inserts).

A

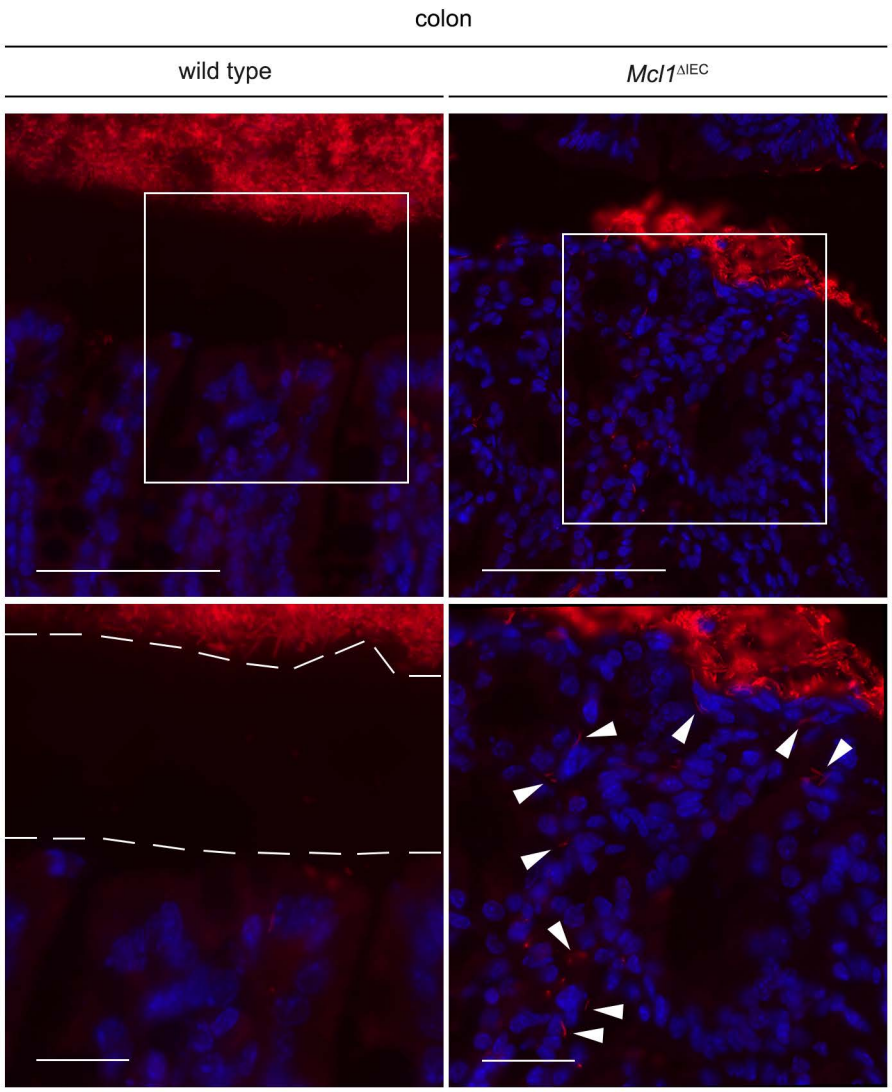

Figure S3. Healy*, Boege*, Hodder* et al.

Figure S3: Characterisation of *Mcl1*$^{\Delta IEC}$ mice. (*A*) Representative images from FISH analysis illustrating *Universal Bacterial 16S* rRNA staining (red) in colon of 2-month-old wild type and *Mcl1*$^{\Delta IEC}$ mice. Dashed lines illustrate the sterile mucosal barrier (intact in wild type mice) preventing bacteria from entering the mucosa. This protective mucosal layer is lost in *Mcl1*$^{\Delta IEC}$ mice. White arrowheads illustrate bacteria that have translocated from the lumen to the mucosal layer via the impaired epithelial barrier in *Mcl1*$^{\Delta IEC}$ mice (scale bars: 100μm scale for top images, 25μm scale for bottom images).

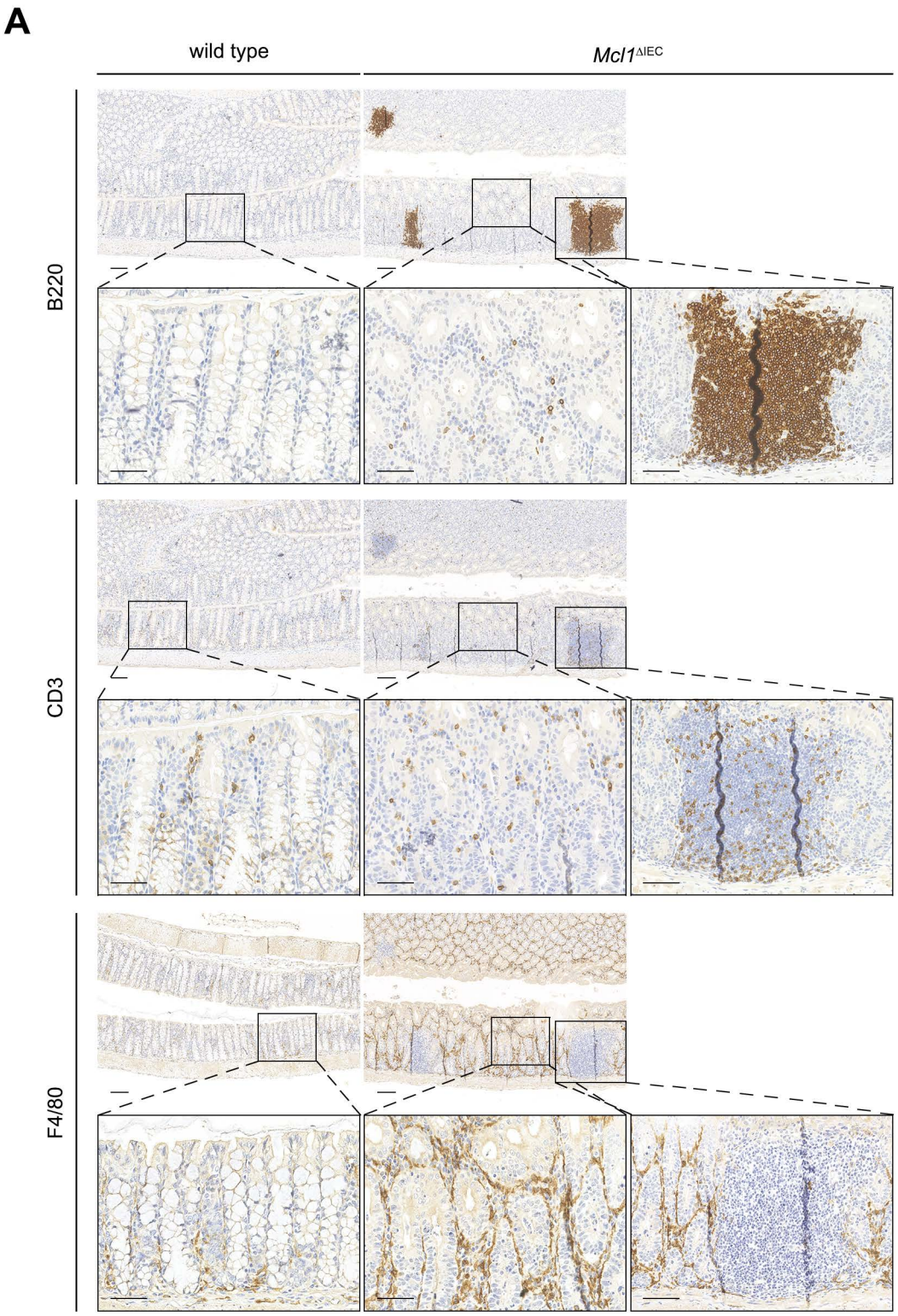

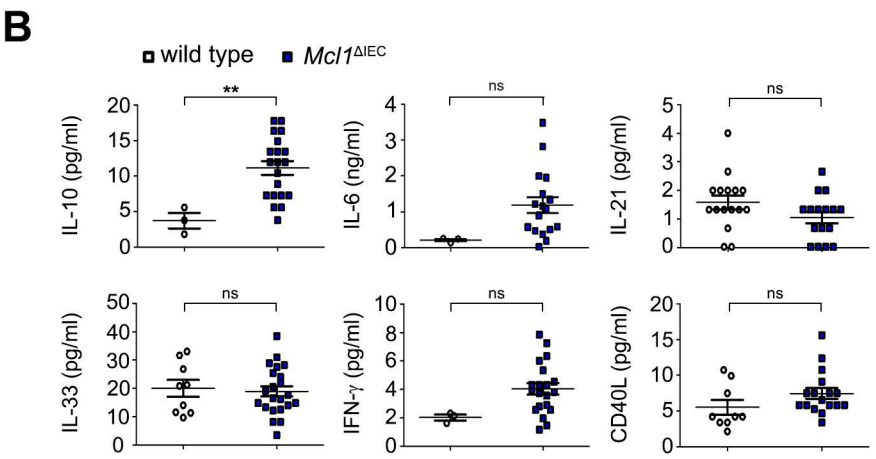

Figure S4. Healy*, Boege*, Hodder* et al.

Figure S4: Characterisation of *Mcl1*$^{\Delta IEC}$ mice. (*A*) Immunohistochemical characterisation of lymphocyte infiltrates in the colon of 2-month-old wild type control mice compared with *Mcl1*$^{\Delta IEC}$ littermates showing increased B cells (B220), T cells (CD3) and macrophages (F4/80) in *Mcl1*$^{\Delta IEC}$ mice. High magnification images show infiltrating immune cells within the lamina propria or lymphoid follicles that were present throughout the small intestine and colon of *Mcl1*$^{\Delta IEC}$ mice (scale bars: 100μm for lower magnification, 50μm for higher magnification images). (*B*) Ex vivo colon cultures established from 2-month-old mice and analysed for IL-10, IL-6, IL-21, IL-33, IFN-γ and CD40L expression using multiplex analysis (minimum n=10 per group). Data presented as scatter plot graphs show individual data points ± s.e.m. Statistical analysis was conducted by one-way ANOVA with Bonferroni correction (*B*) where ** $p \leq 0.01$.

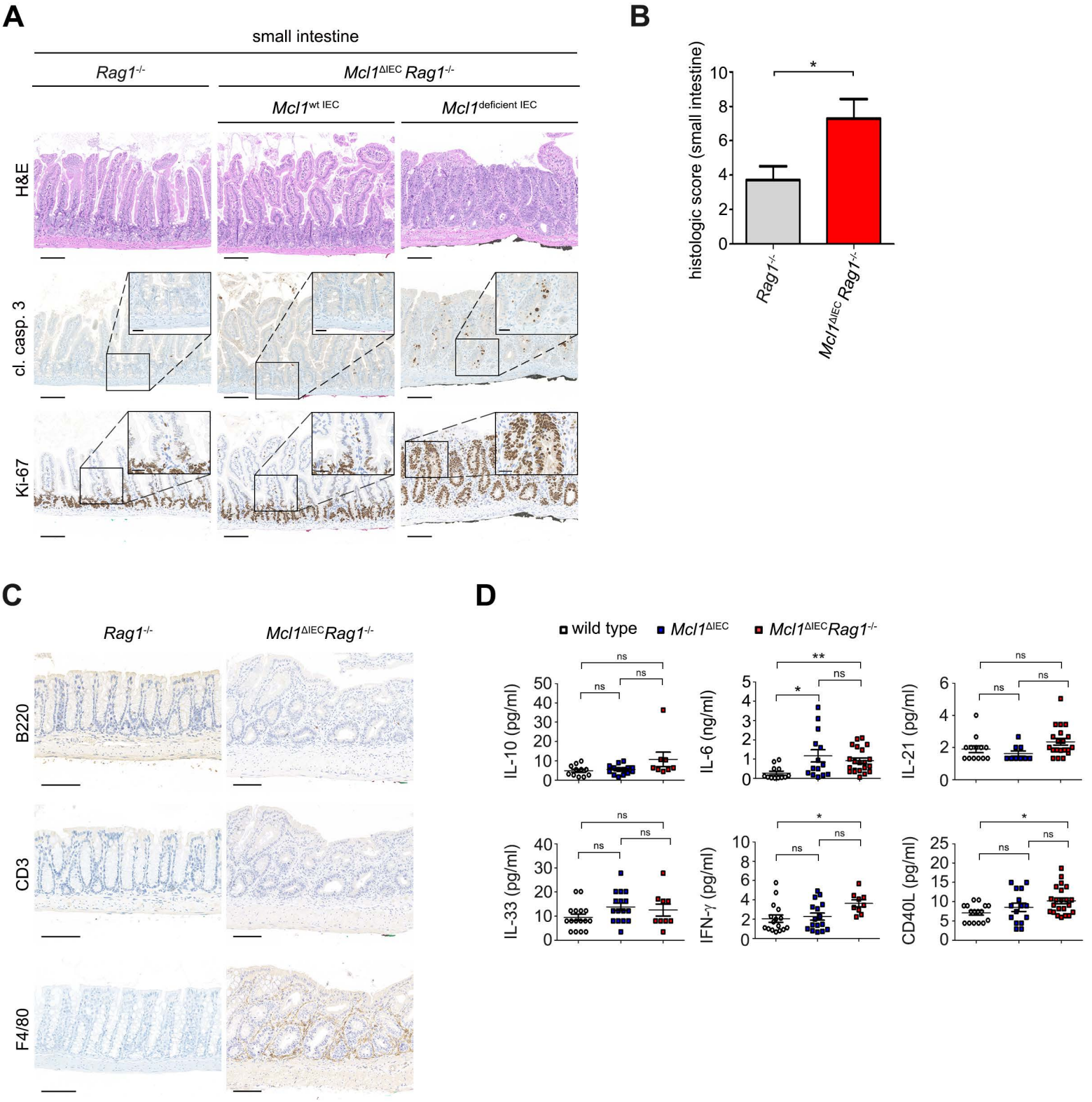

Figure S5. Healy*, Boege*, Hodder* et al.

Figure S5: Inflammation in *Mcl1*$^{\Delta IEC}$ mice is independent of T and B cells. (*A*) Representative images from the small intestine from 2-month-old *Rag1*$^{-/-}$ control mice compared with age-matched *Mcl1*$^{\Delta IEC}$*Rag1*$^{-/-}$ mice illustrating impaired intestinal architecture (H&E), increased IEC apoptosis (cl. casp. 3) and hyperproliferation (Ki-67) (scale bars: 100μm, 25μm for inserts). (*B*) Blinded histological score of small intestine samples from 2-month-old *Mcl1*$^{\Delta IEC}$*Rag1*$^{-/-}$ mice compared with age-matched *Rag1*$^{-/-}$ control mice show significantly increased pathology in *Mcl1*$^{\Delta IEC}$*Rag1*$^{-/-}$ mice (n=5). (*C*) 2-month-old *Rag1*$^{-/-}$ control mice and age-matched *Mcl1*$^{\Delta IEC}$*Rag1*$^{-/-}$ mice were stained for B cell (B220), T cell (CD3) and macrophage (F4/80) expression using IHC to confirm the lack of mature T and B cells (scale bar: 100μm). (*D*) Ex vivo colon cultures were established from 2-month-old mice and analysed for IL-10, IL-6, IL-21, IL-33, IFN-γ and CD40L expression using multiplex analysis (minimum n=9 per group). Data presented as either bar charts or scatter plot graph show mean values ± s.e.m. Statistical analyses were conducted by Mann-Whitney test (*B*) or one-way ANOVA with Bonferroni correction (*D*) where * $p \leq 0.05$, ** $p \leq 0.01$.

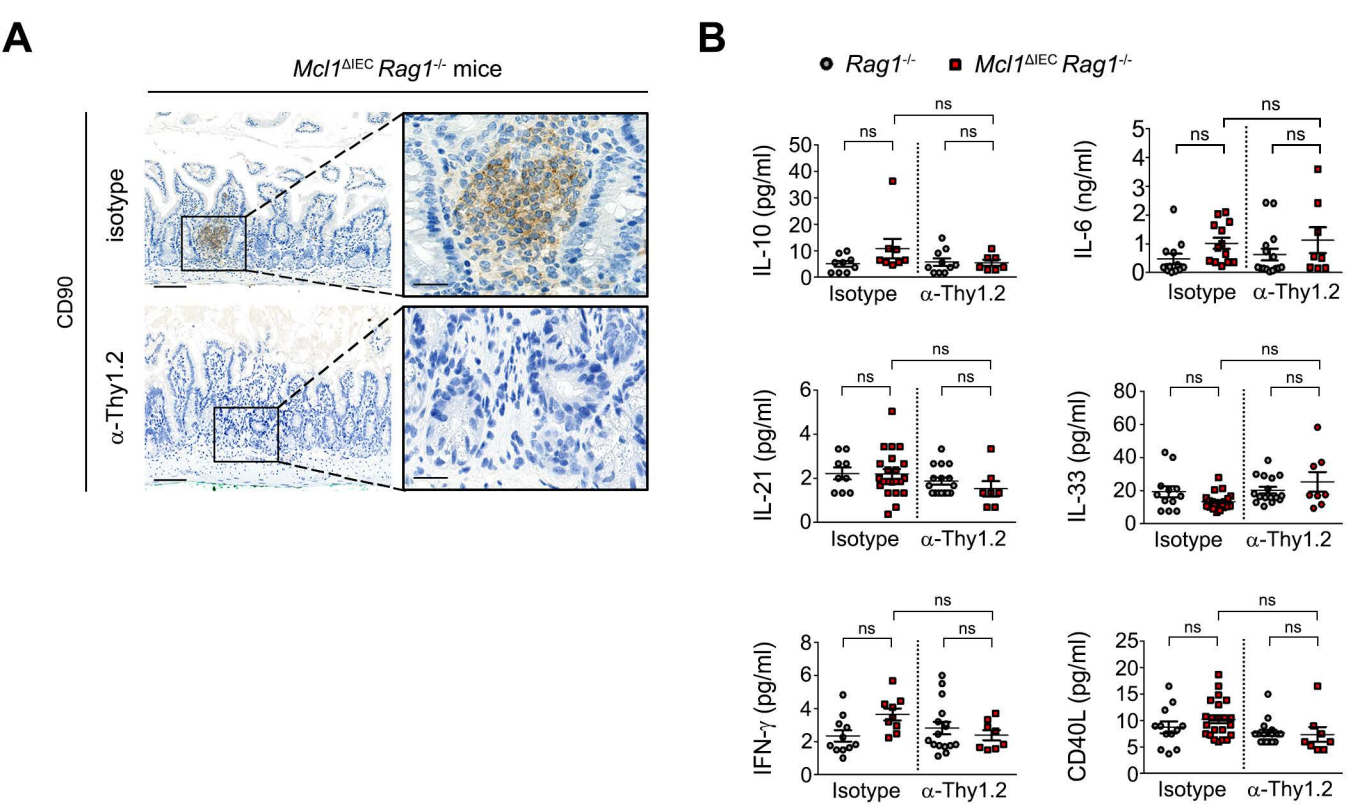

Figure S6. Healy*, Boege*, Hodder* et al.

Figure S6: ILC depletion eliminates pro-inflammatory cytokine production. (*A*) 2-month-old *Mcl1*$^{\Delta IEC}$*Rag1*$^{-/-}$ mice were treated with either isotype control or α-Thy1.2 depleting antibody for 4 weeks. Immunohistochemistry shows CD90 (Thy1) positive cells in the 3-month-old isotype control treated mice, which are not present in the mice that received α-Thy1.2 depleting antibody, thus indicating efficient depletion of ILC (scale bars: 100μm (left images), 25μm (right images)). (*B*) Ex vivo colon cultures established from 3-month-old mice and analysed for IL-10, IL-6, IL-21, IL-33, IFN-γ and CD40L expression using multiplex analysis (minimum n=8 per group). Data presented as scatter plot graph show mean values ± s.e.m. Statistical analysis was conducted by one-way ANOVA with Bonferroni correction (*B*).

A

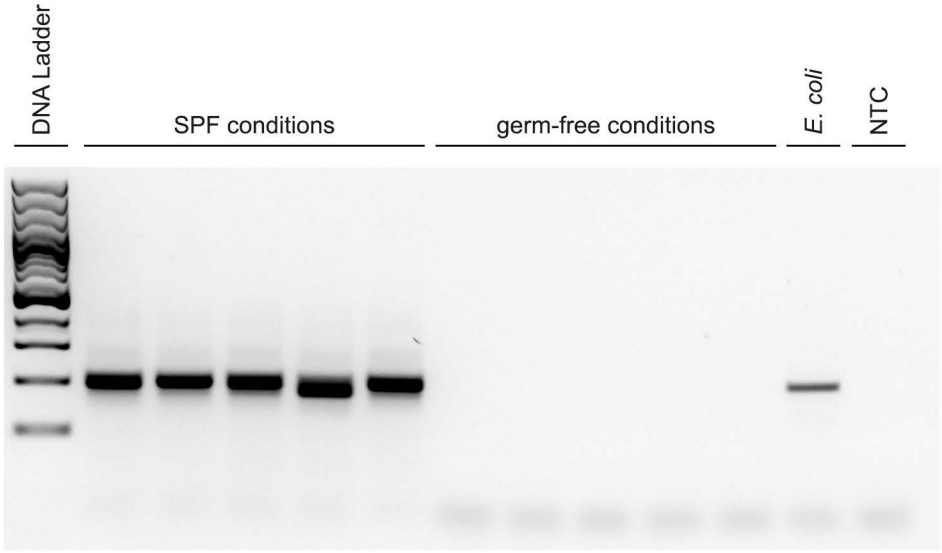

B

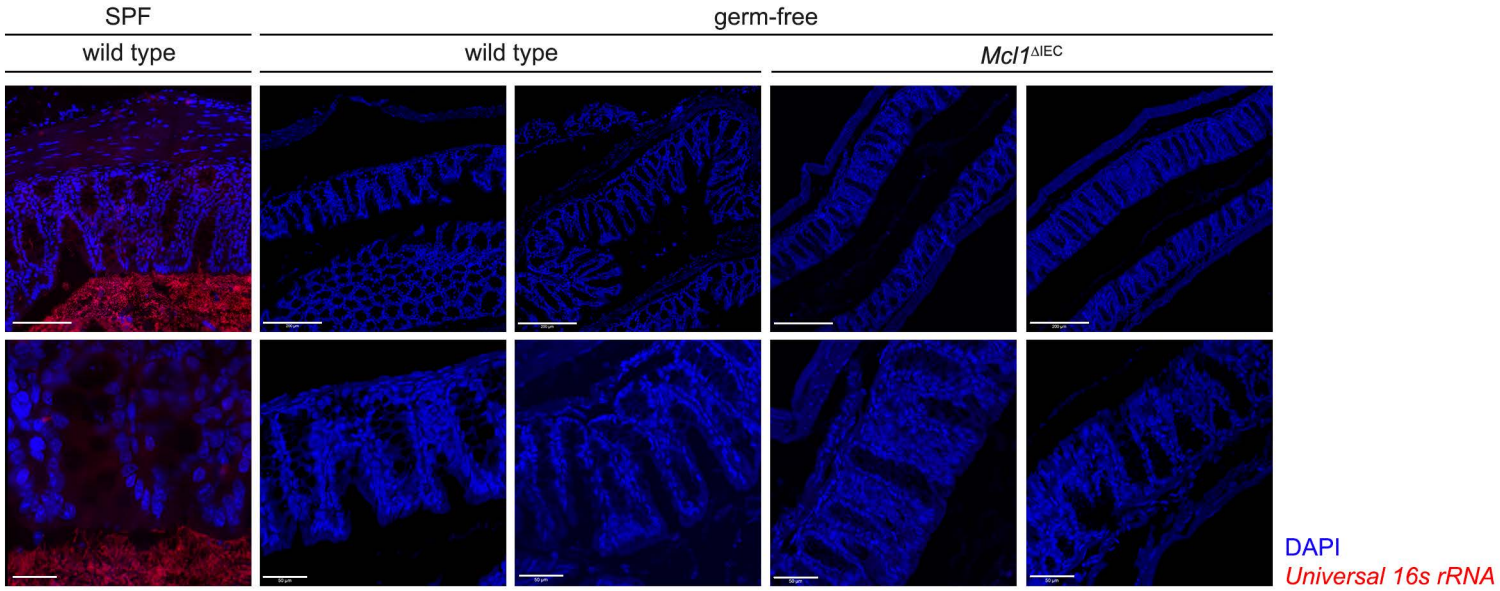

Figure S7. Healy*, Boege*, Hodder* et al.

Figure S7: *Mcl1*$^{\Delta IEC}$ raised under germ-free conditions are completely void of commensal bacteria. (*A*) PCR analysis showing the presence of bacterial 16s DNA isolated from the faeces of wild type and *Mcl1*$^{\Delta IEC}$ mice raised under SPF conditions. Samples isolated from the faeces of wild type and *Mcl1*$^{\Delta IEC}$ mice raised under germ-free conditions showed no bacterial 16s. *E. coli* was used as a positive control. NTC: no-template control. (*B*) Representative images from FISH analysis illustrating Universal Bacterial 16S rRNA staining (red) in colon of a 2-month-old wild type control mouse raised under SPF conditions. No positive FISH signal was recorded in either wild type control mice or *Mcl1*$^{\Delta IEC}$ mice raised under germ-free conditions (scale bars: 200μm top images, 50μm for bottom images).

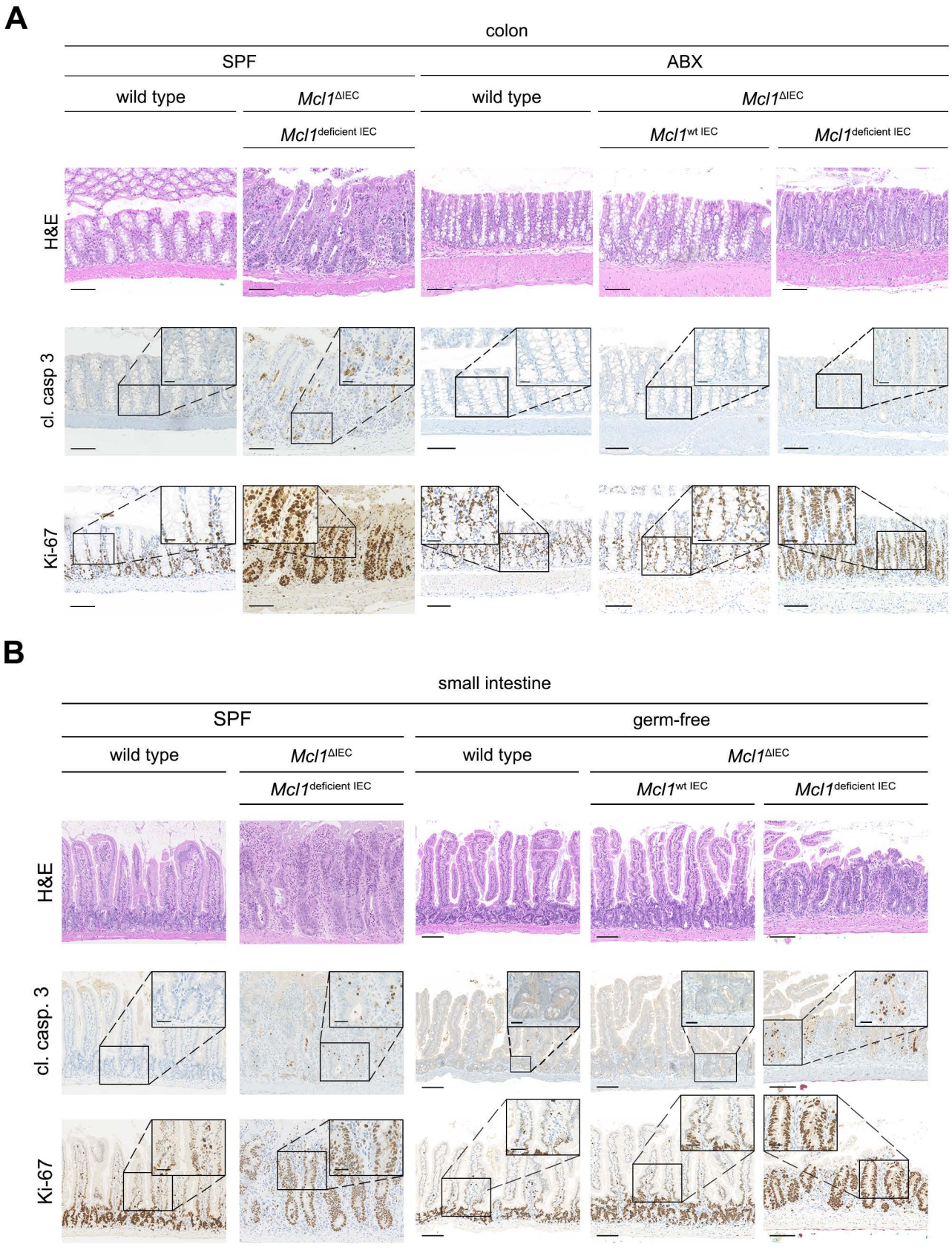

Figure S8. Healy*, Boege*, Hodder* et al.

Figure S8: Increased apoptosis, hyperproliferation and impaired differentiation are a direct consequence of MCL1 deficiency. (*A*) Representative images taken from colons of 2-month-old wild type and *Mcl1*$^{\Delta IEC}$ mice following ABX treatment illustrating retained IEC apoptosis (cl. casp 3) and hyperproliferation (Ki-67) (scale bars 100μm, 25μm for inserts). (*B*) Representative images from the small intestine from 2-month-old germ-free wild type control mice compared with germ-free *Mcl1*$^{\Delta IEC}$ mice illustrating that increased apoptosis (cl. casp. 3) and hyperproliferation (Ki-67) caused by MCL1 deficiency are also observed under germ-free conditions (scale bars: 100μm, 25μm for inserts). (*C*) Blinded histological scoring illustrating significantly reduced histological score in the small intestine of ABX treated 2-month-old *Mcl1*$^{\Delta IEC}$ mice and 2-month-old germ-free *Mcl1*$^{\Delta IEC}$ mice compared with age-matched *Mcl1*$^{\Delta IEC}$ mice housed under SPF conditions (n=5). (*D*) Representative images illustrating the defective intestinal epithelial barrier in *Mcl1*$^{\Delta IEC}$ mice, irrespective of whether these mice were housed under SPF or germ-free conditions (scale bars: 100μm for top images, 25μm for bottom). Data presented as scatter plot graph show mean values ± s.e.m. Statistical analyses were evaluated by Mann-Whitney test (*C*) where * $p \leq 0.05$.

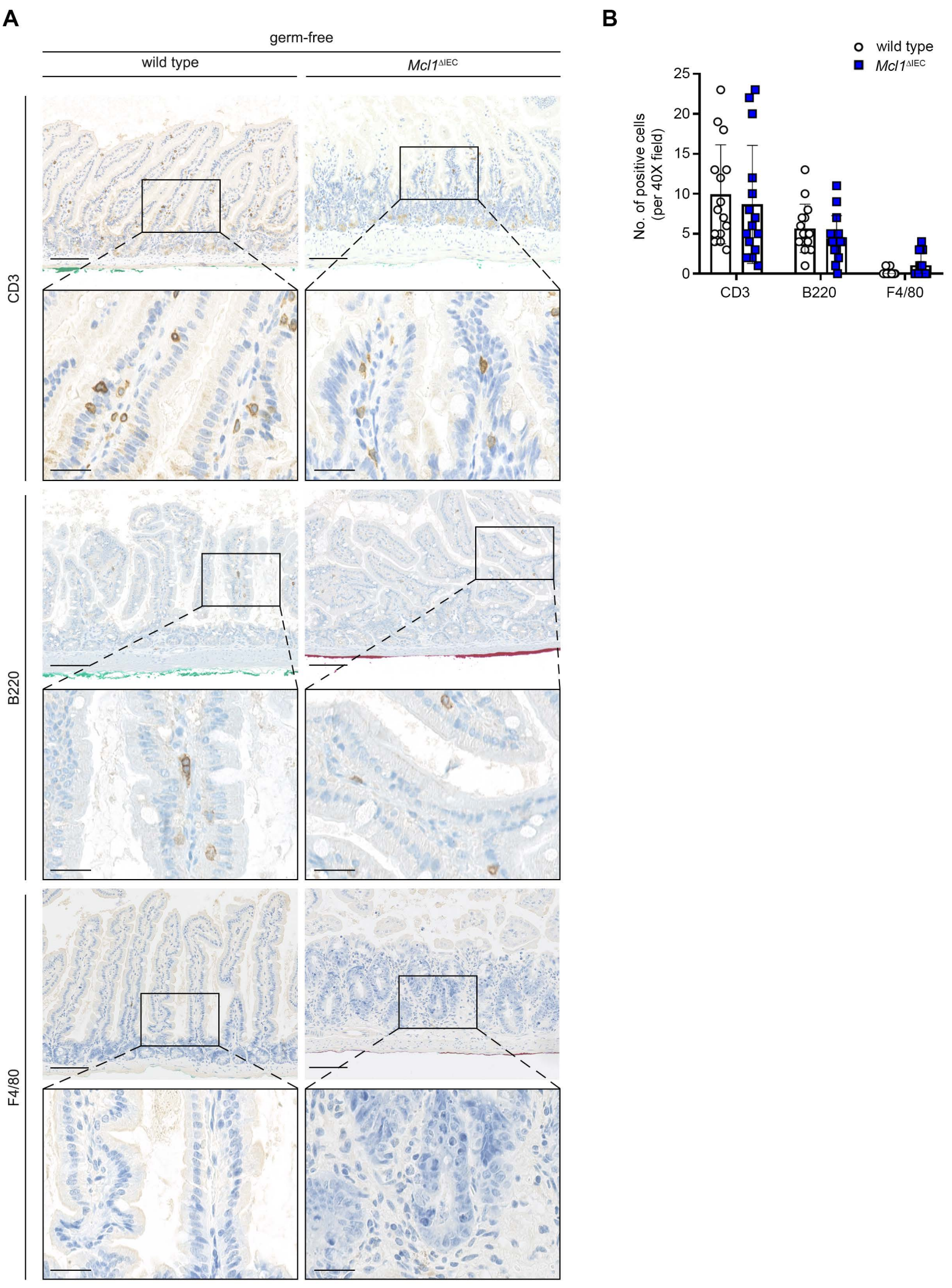

Figure S9. Healy*, Boege*, Hodder* et al.

Figure S9: *Mcl1* deletion does not result in intestinal inflammation under germ-free conditions. (*A*) Immunohistochemical characterisation of lymphocytes in the colon of 2-month-old germ-free wild type control mice compared with *Mcl1*$^{\Delta IEC}$ littermates showing no increase in infiltrating T cells (CD3), B cells (B220) or macrophages (F4/80) in germ-free *Mcl1*$^{\Delta IEC}$ mice (scale bar: 100μm). (*B*) Quantification of infiltrating T cells, B cells and macrophages in germ-free *Mcl1*$^{\Delta IEC}$ mice compared with littermate controls. Data presented as scatter plot graph show mean values ± s.e.m. Statistical analyses were evaluated by Mann-Whitney test (*B*).

A

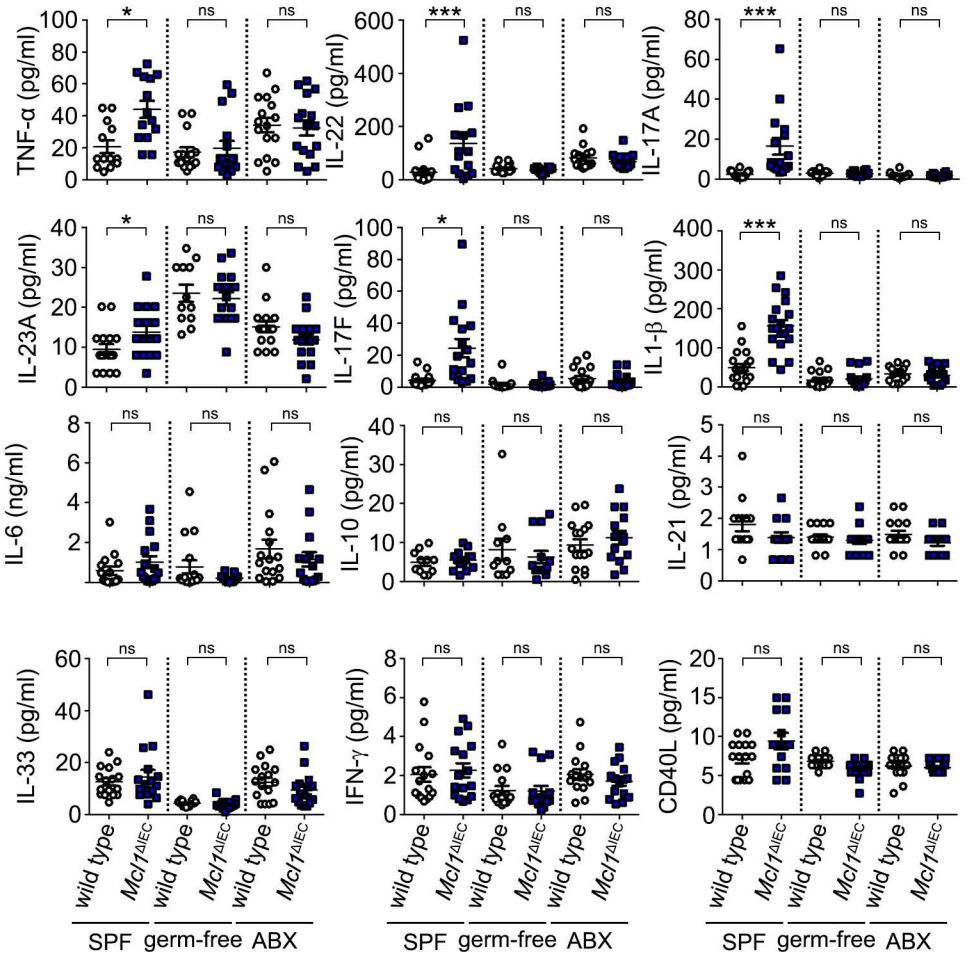

Figure S10. Healy*, Boege*, Hodder* et al.

Figure S10: Chronic inflammation observed in *Mcl1*$^{\Delta IEC}$ mice is an immune response against disseminating commensal bacteria. (*A*) Ex vivo colon cultures were established from 2-month-old mice and analysed for TNF-α, IL-22, IL-23A, IL17A, IL-17F, IL-1β, IL-10, IL-6, IL-21, IL-33, IFN-γ and CD40L expression using multiplex analysis (minimum n=12 per group). Data presented as scatter plot graph show mean values ± s.e.m. Statistical analyses were evaluated by one-way ANOVA with Bonferroni correction (*A*) where * $p \leq 0.05$, ** $p \leq 0.01$, *** $p \leq 0.001$.

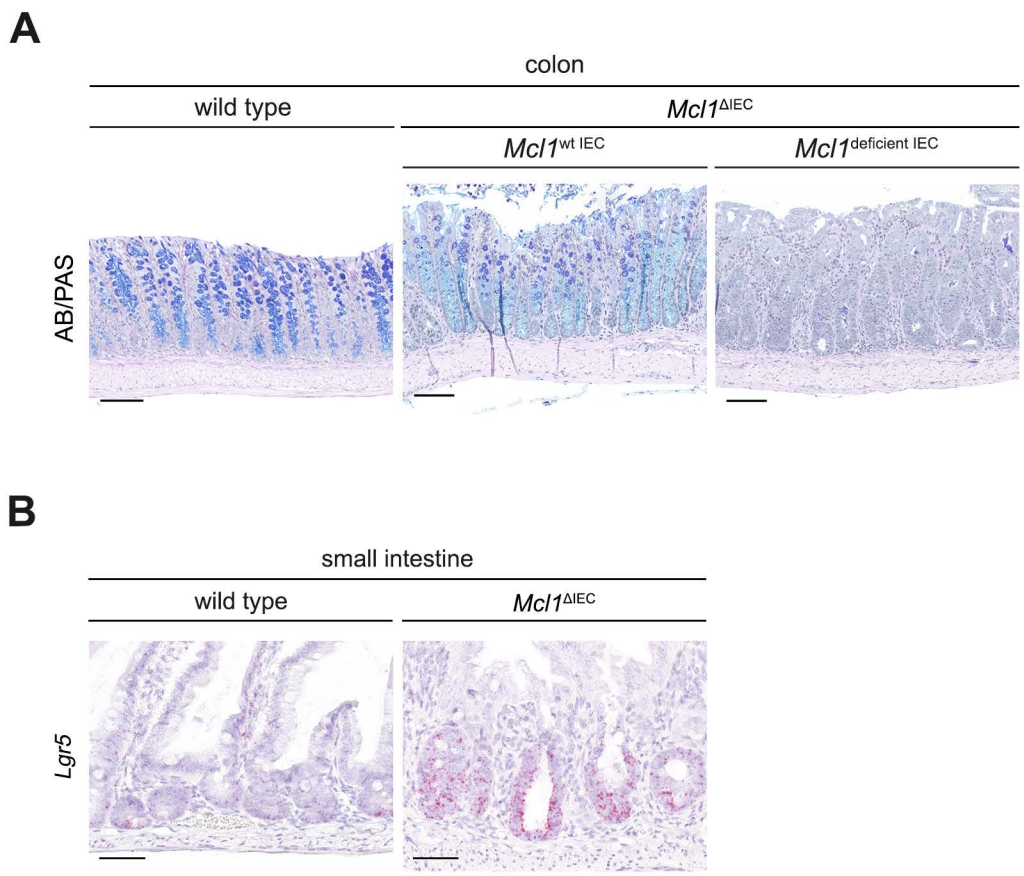

Figure S11. Healy*, Boege*, Hodder* et al.

Figure S11: MCL1 is essential for ISC differentiation to secondary secretory lineages and protection from DNA damage. (*A*) Representative images taken from colons of 2-month-old wild type and *Mcl1*$^{\Delta IEC}$ mice illustrating the impaired ISC differentiation to goblet cells (AB/PAS) (scale bar: 100μm). (*B*) Representative images from the small intestine from 2-month-old germ-free wild type control mice compared with *Mcl1*$^{\Delta IEC}$ littermate mice illustrating expansion of the *Lgr5*+ ISC compartment by *in situ* hybridization (scale bar: 50μm).

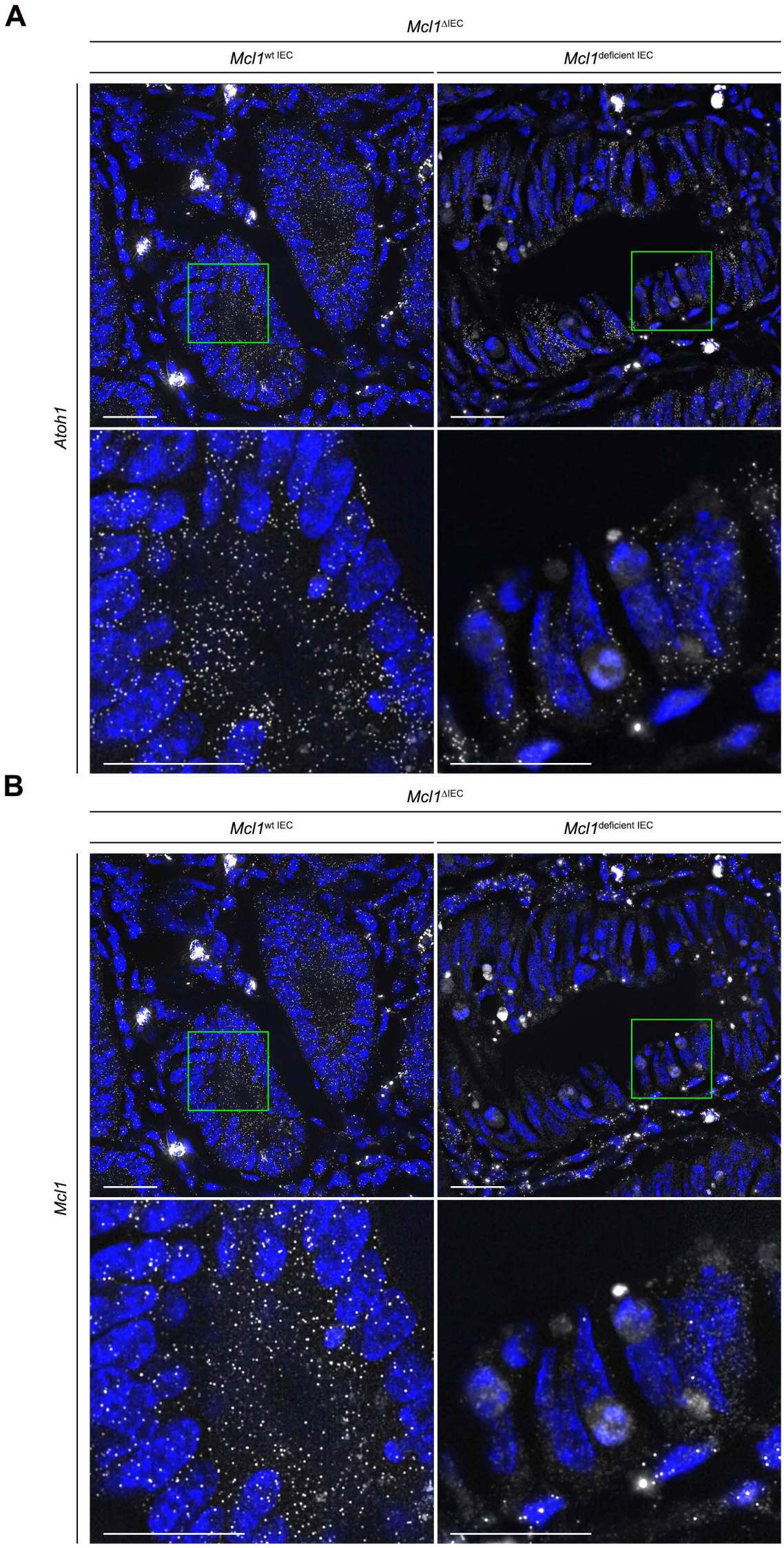

Figure S12. Healy*, Boege*, Hodder* et al.

Figure S12: *Mcl1* deficiency correlates with a marked reduction of *Atoh1* expression in intestinal crypts. (*A*) Corresponding single colour control images from Figure 4*D*. *Atoh1* expression levels in *Mcl1*-positive versus *Mcl1*-deficient IEC visualized using smFISH. White dots represents single molecules of *Atoh1.* Green boxes mark the areas shown in higher magnification in the image directly below (scale bars: 25μm for top images, 10μm for bottom images). (*B*) Corresponding single colour control images from Figure 4*D*. *Mcl1* expression levels in *Mcl1*-positive versus *Mcl1*-deficient IEC visualized using smFISH. White dots represents single molecules of *Mcl1.* Green boxes mark the areas shown in higher magnification in the image directly below (scale bars 25μm for top images, 10μm for bottom images).

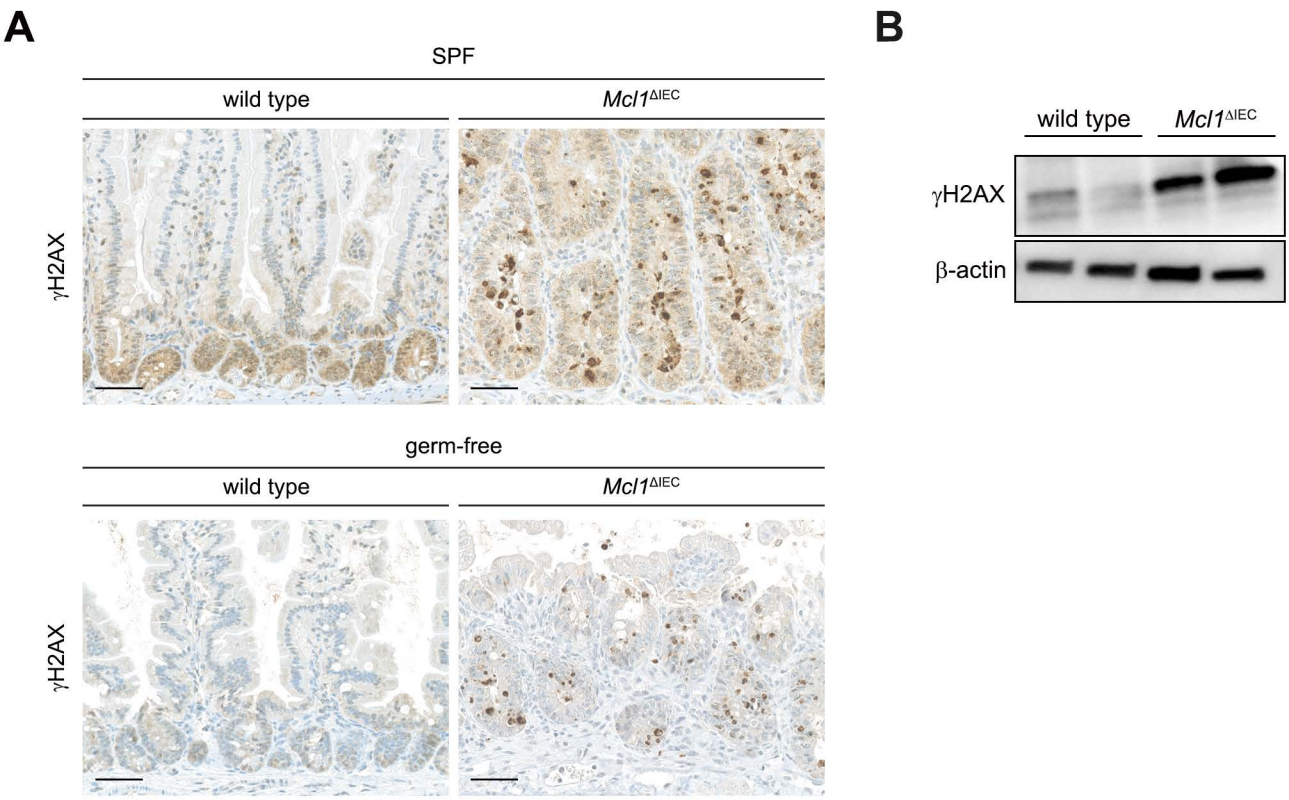

Figure S13. Healy*, Boege*, Hodder* et al.

Figure S13: Mcl1 protects IEC from the accumulation of DNA damage. (*A*) IHC comparing γH2AX positivity in 2-month-old *Mcl1*$^{\Delta IEC}$ mice with littermate controls (scale bar: 50μm). (*B*) Western blot analysis corroborating the marked increase in γH2AX levels in *Mcl1*$^{\Delta IEC}$ mice compared to littermate controls.

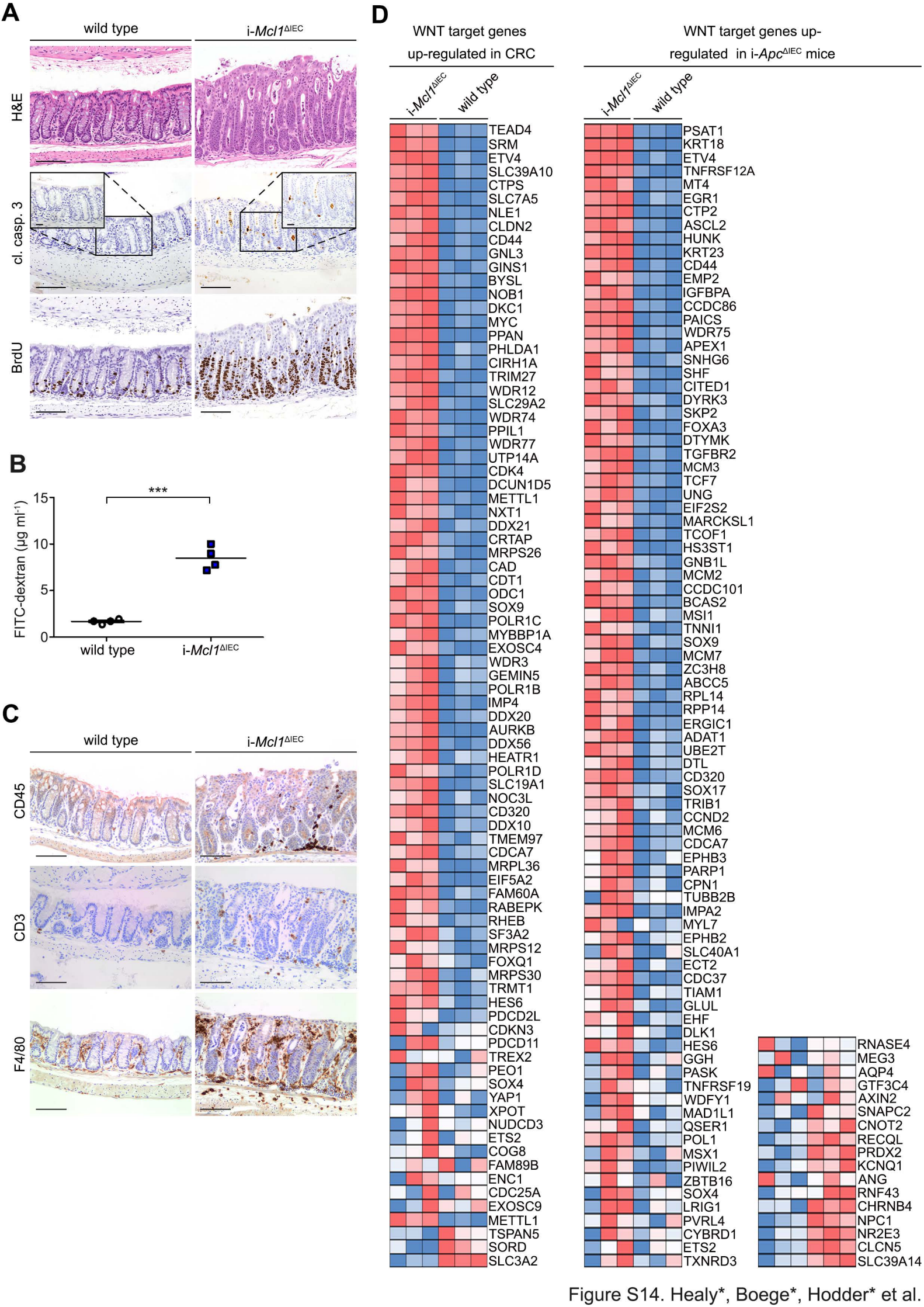

Figure S14. Healy*, Boege*, Hodder* et al.

Figure S14: IEC MCL1 deficiency results in activation of WNT signalling pathways. (*A*) Representative images from the colon of wild type control and i-*Mcl1*$^{\Delta IEC}$ mice showing crypt hyperplasia (H&E), increased apoptosis (cl. casp. 3) and hyper-proliferation (BrdU) in i-*Mcl1*$^{\Delta IEC}$ mice sampled 4 days post induction, mirroring results observed in the *Mcl1*$^{\Delta IEC}$ mice (scale bars: 100μm, 25μm for insert). (*B*) Serum analysis indicating increased FITC-dextran i-*Mcl1*$^{\Delta IEC}$ mice compared with age-matched wild type controls 4 hours after oral administration (2 days after induction, n=4). (*C*) Immunohistochemical characterisation of lymphocyte infiltrates in the colon of wild type control mice compared with i-*Mcl1*$^{\Delta IEC}$ littermates showing increased lymphocytes (CD45), T cells (CD3) and macrophages (F4/80) in the lamina propria of i-*Mcl1*$^{\Delta IEC}$ mice (2 days after induction) (scale bars: 100μm). (*D*) Expression of genes as analysed by RNA sequencing of small intestine tissue from i-*Mcl1*$^{\Delta IEC}$ mice compared with wild type control mice illustrated in heat maps and captured in the GSEA signatures. WNT target genes commonly upregulated in human CRC (left), and genes enriched in i-*Apc*$^{\Delta IEC}$ mice (right). Red boxes represent high expression while blue boxes represent low expression. Data presented as scatter plot graph represents mean values ± s.e.m. Statistical analysis was conducted by Mann-Whitney test (*B*) where *** $p \leq 0.001$.

A

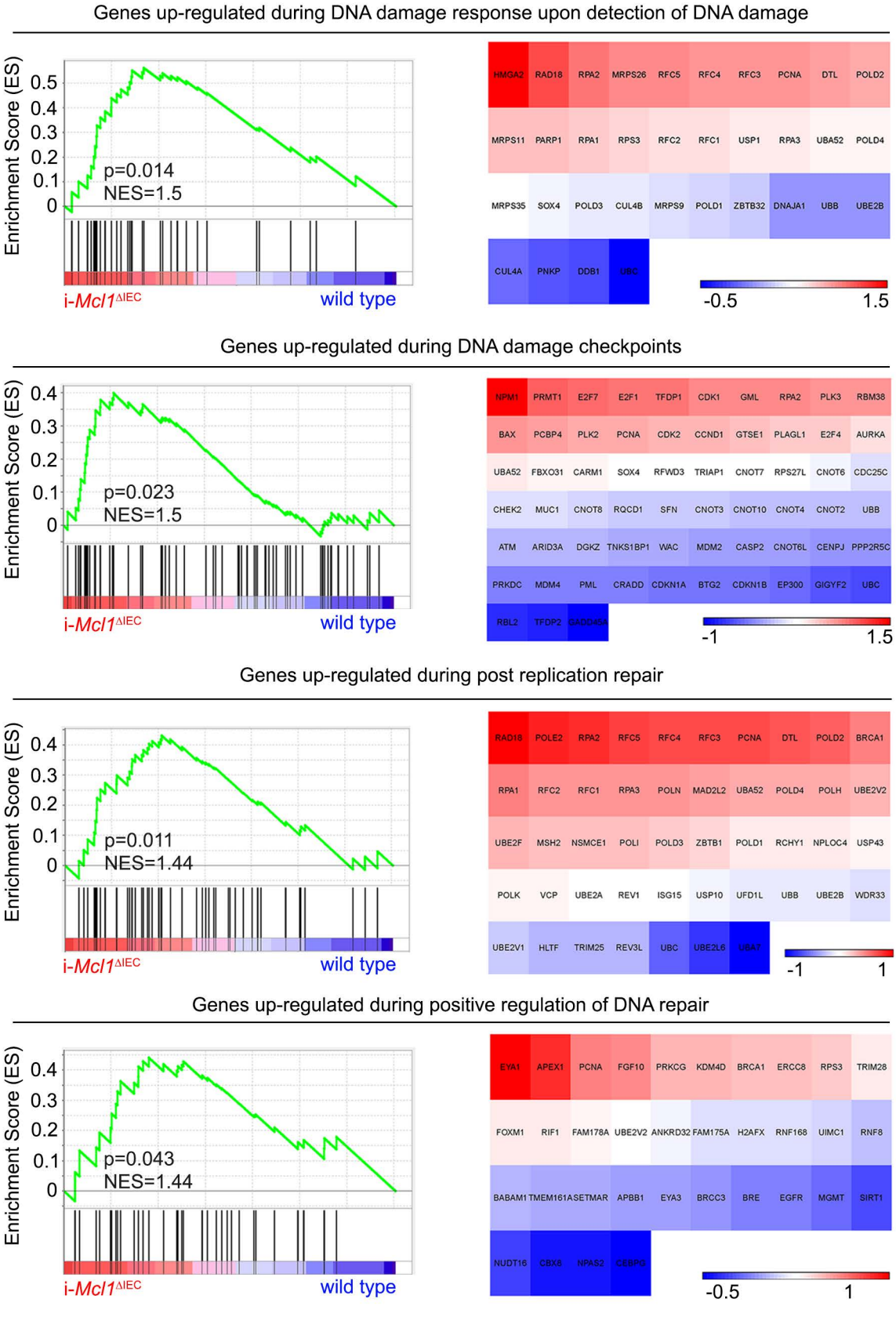

Figure S15. Healy*, Boege*, Hodder* et al.

Figure S15: IEC MCL1 deficiency results in up-regulation of DNA damage associated genes. (*A*) GSEA plots derived from G0 term gene sets by RNA sequencing analysis of small intestine tissue from i-*Mcl1*$^{\Delta IEC}$ mice (samples 3 days after induction) compared with wild type control mice and corresponding heat maps illustrating increased expression of DNA damage response associated gene sets in i-*Mcl1*$^{\Delta IEC}$ mice. Red boxes represent increased expression while blue boxes represent reduced expression (gene expression values are presented as log2 ratios).

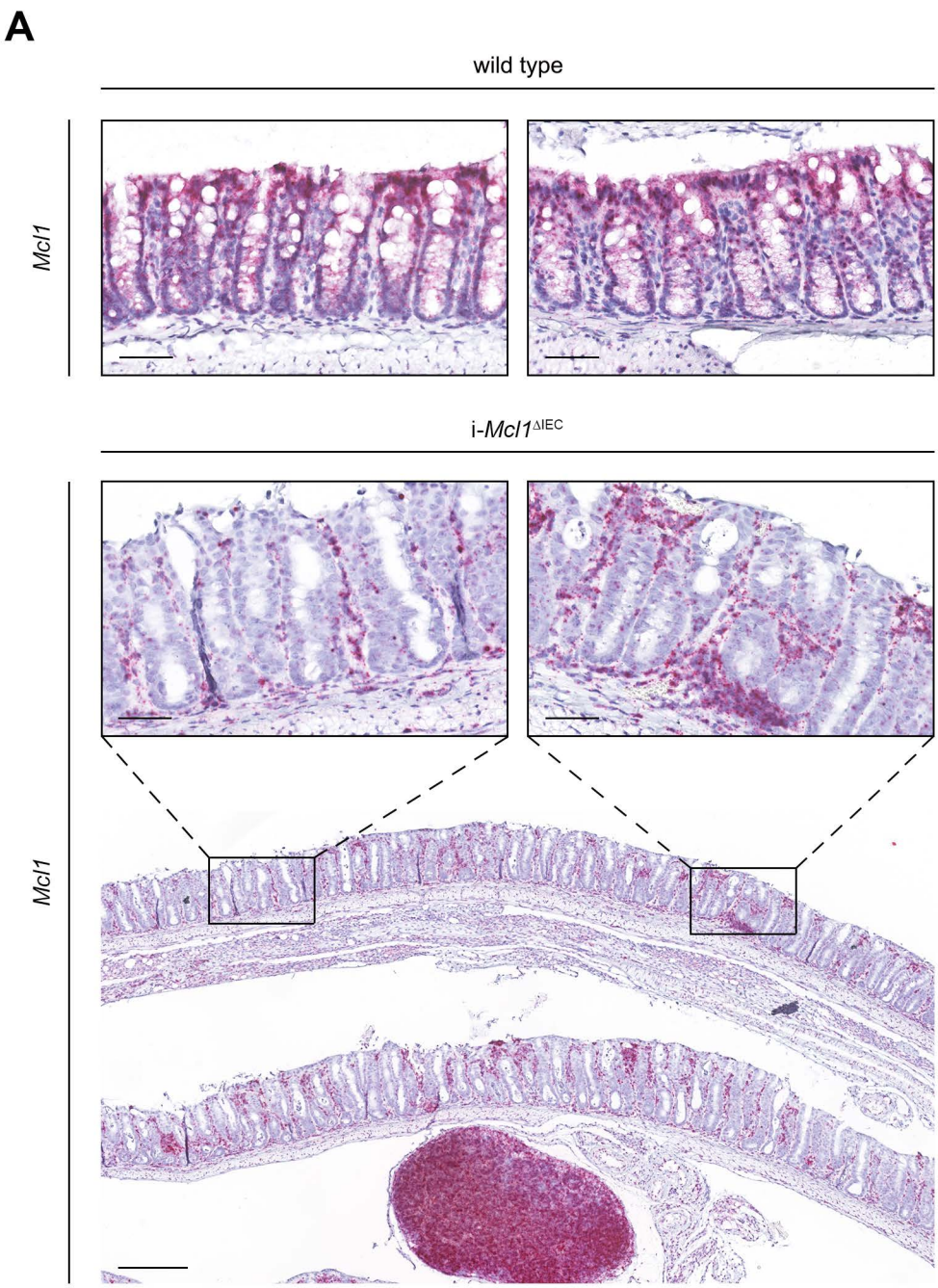

Figure S16. Healy*, Boege*, Hodder* et al.

Figure S16: i-*Mcl1*$^{\Delta IEC}$ mice show complete recombination of *Mcl1* throughout the entire intestinal tract. (A) Representative images illustrating *Mcl1* expression in the colon (red stain) of non-recombined wild type control mice (top panel) compared to i-*Mcl1*$^{\Delta IEC}$ mice (lower panel) as demonstrated using *in situ* hybridization (scale bars: 250μm for low magnification image, 50 μm for high magnification images).

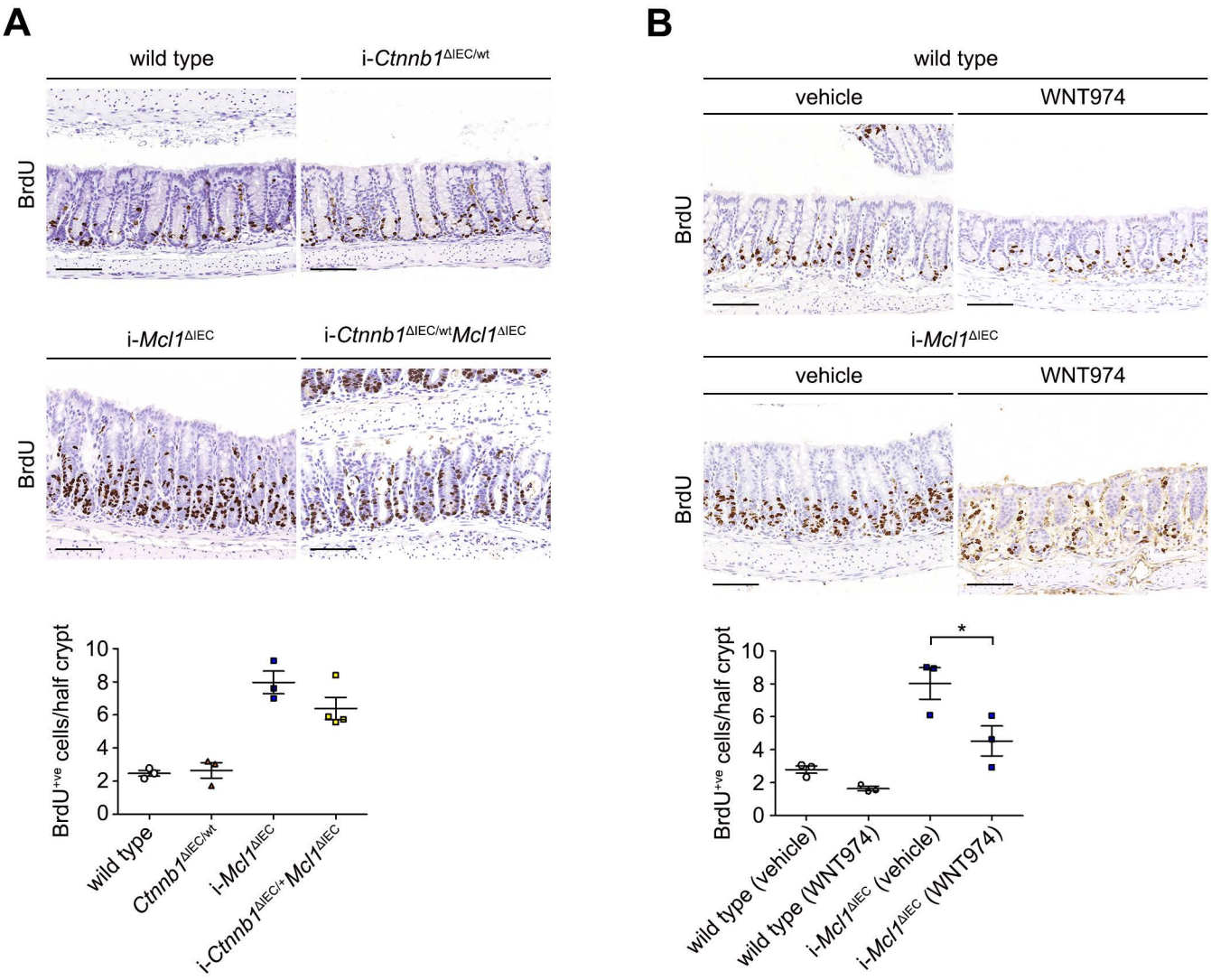

Figure S17. Healy*, Boege*, Hodder* et al.

Figure S17: MCL1 deficiency-induced hyperproliferation is dependent on WNT signaling. (*A*) BrdU staining from the colon of wild type, i-*Ctnnb1*$^{\Delta IEC/+}$, i-*Mcl1*$^{\Delta IEC}$ and i-*Mcl1*$^{\Delta IEC}$*Ctnnb1*$^{\Delta IEC/+}$ mice, sampled 4 days after induction, indicating increased epithelial cell proliferation following *Mcl1* deletion is partially rescued in i-*Mcl1*$^{\Delta IEC}$*Ctnnb1*$^{\Delta IEC/+}$ mice (scale bars: 100μm). Quantitative analysis of BrdU positive cells/half crypt is shown below (n=3 or 4 per group). (*B*) BrdU staining from the colons of vehicle treated wild type and i-*Mcl1*$^{\Delta IEC}$ mice compared with WNT974 treated wild type and i-*Mcl1*$^{\Delta IEC}$ mice, sampled 3 days post induction, (scale bars: 100μm) as well as quantitative analysis of BrdU positive cells/half crypt illustrating inhibition of epithelial cell proliferation following WNT974 treatment (n=3 per group) (below). Data presented as scatter plot graph represents mean values ± s.e.m. Statistical analysis was conducted by Mann-Whitney test (*A*-*B*) where * $p \leq 0.05$.

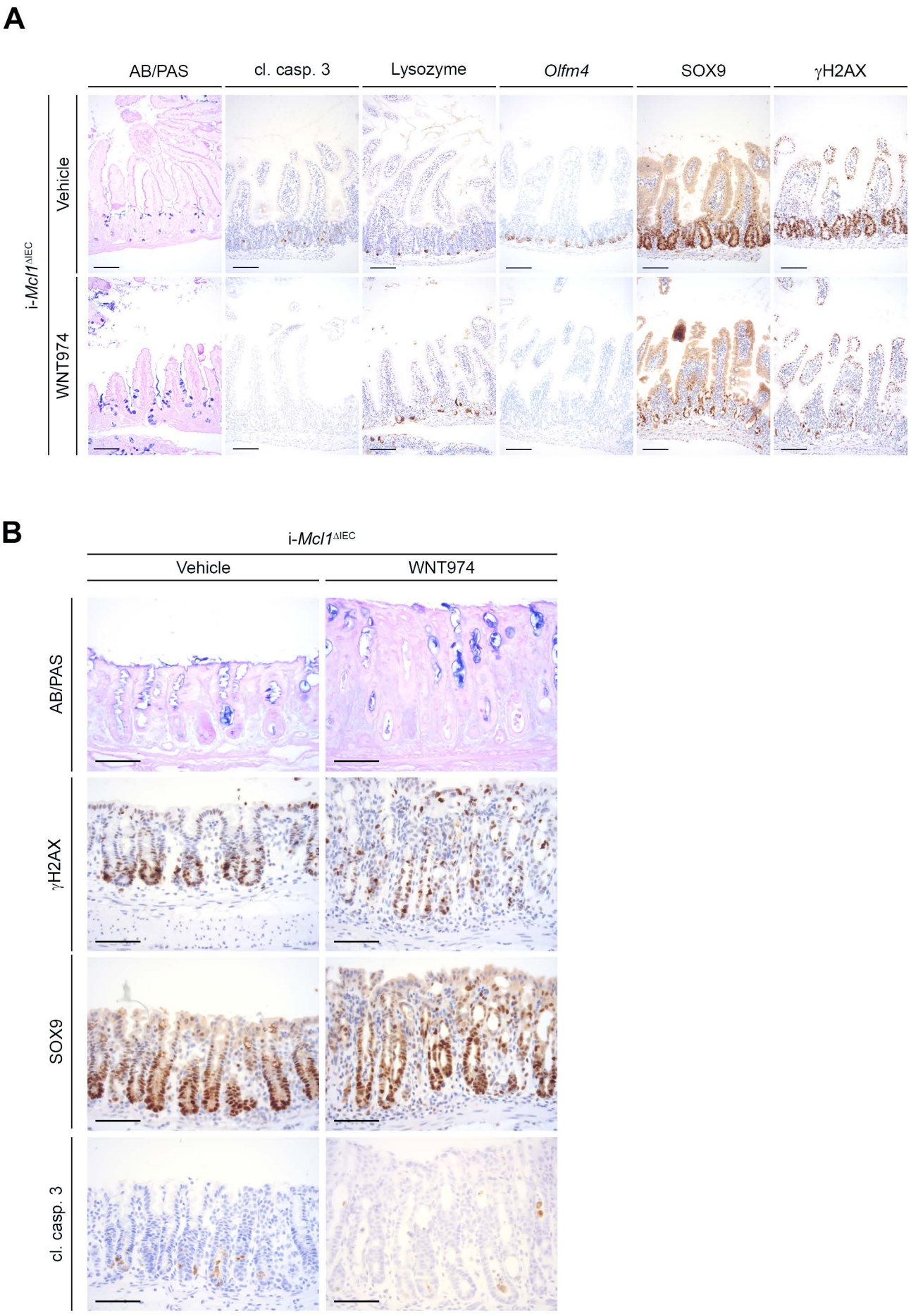

Figure S18. Healy*, Boege*, Hodder* et al.

Figure S18: MCL1-deficiency induced hyperproliferation is dependent on WNT signaling. (*A*) Representative images from the small intestine of wild type control and i-*Mcl1*$^{\Delta IEC}$ mice following treatment with WNT974 or vehicle control, 3 days post induction. Images show the effect of WNT974 on ISC differentiation (AB/PAS, Lysozyme), apoptosis (cl. caps. 3), ISC populations (*Olfm4*, SOX9) and DNA damage (γH2AX) (scale bars: 100μm). (*B*) Representative images from the colon of wild type control and i-*Mcl1*$^{\Delta IEC}$ mice following treatment with WNT974 or vehicle control, 3 days post induction. Images show the effect of WNT974 on ISC differentiation (AB/PAS), apoptosis (cl. caps. 3), ISC populations (SOX9) and DNA damage (γH2AX) (scale bars: 100μm).

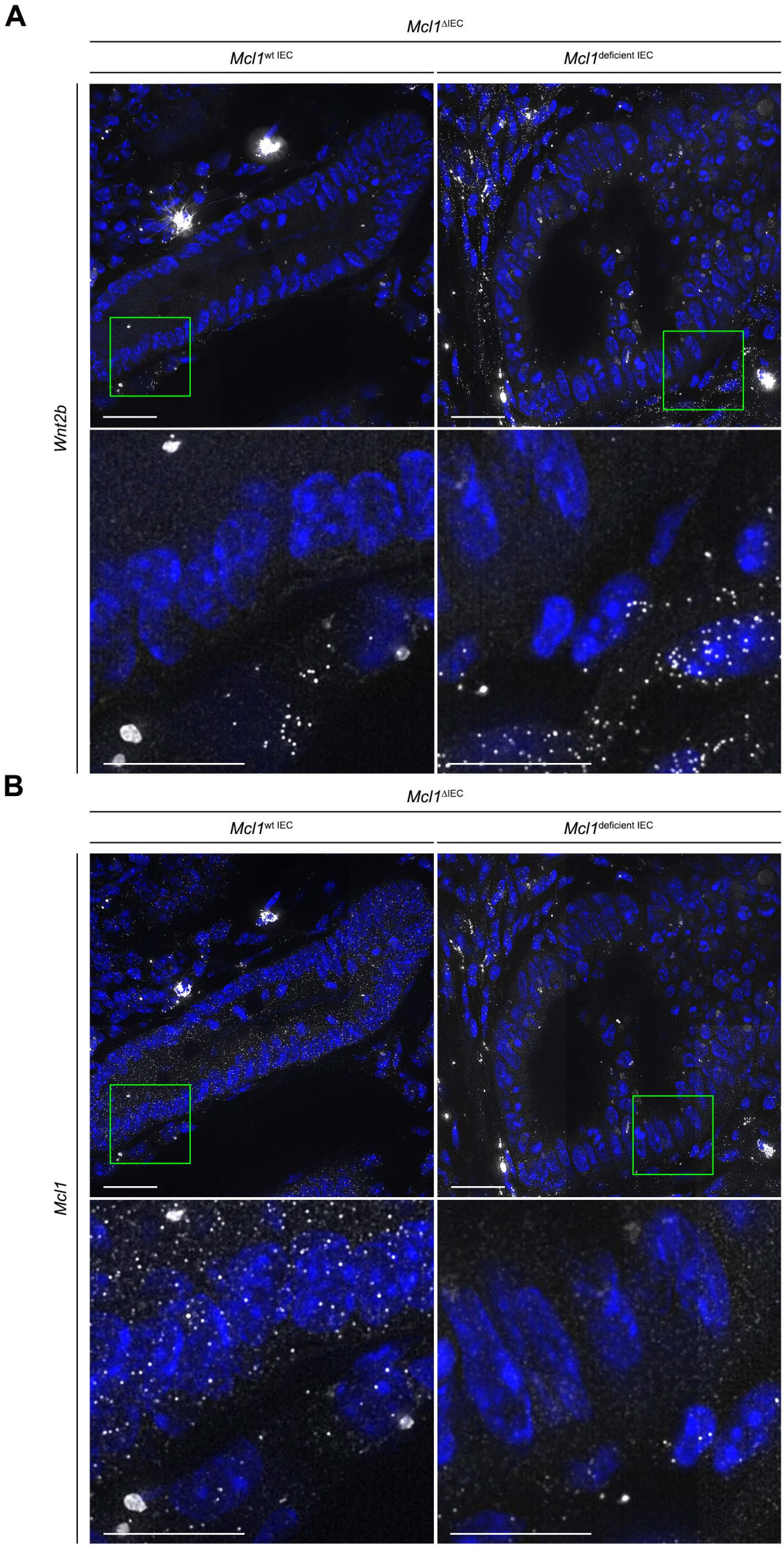

Figure S19. Healy*, Boege*, Hodder* et al.

Figure S19: Increased *Wnt2b* expression is not directly linked to *Mcl1* deficiency. (*A*) Corresponding single colour control images from Figure 5*G*. *Wnt2b* expression levels in *Mcl1*-positive versus *Mcl1*-deficient IEC visualized using smFISH. White dots represents single molecules of *Atoh1.* Green boxes mark the areas shown in higher magnification in the image directly below (scale bars: 25μm for top images, 10μm for bottom images). (*B*) Corresponding single colour control images from Figure 5*G*. *Mcl1* expression levels in *Mcl1*-positive versus *Mcl1*-deficient IEC visualized using smFISH. White dots represents single molecules of *Mcl1.* Green boxes mark the areas shown in higher magnification in the image directly below (scale bars: 25μm for top images, 10μm for bottom images).

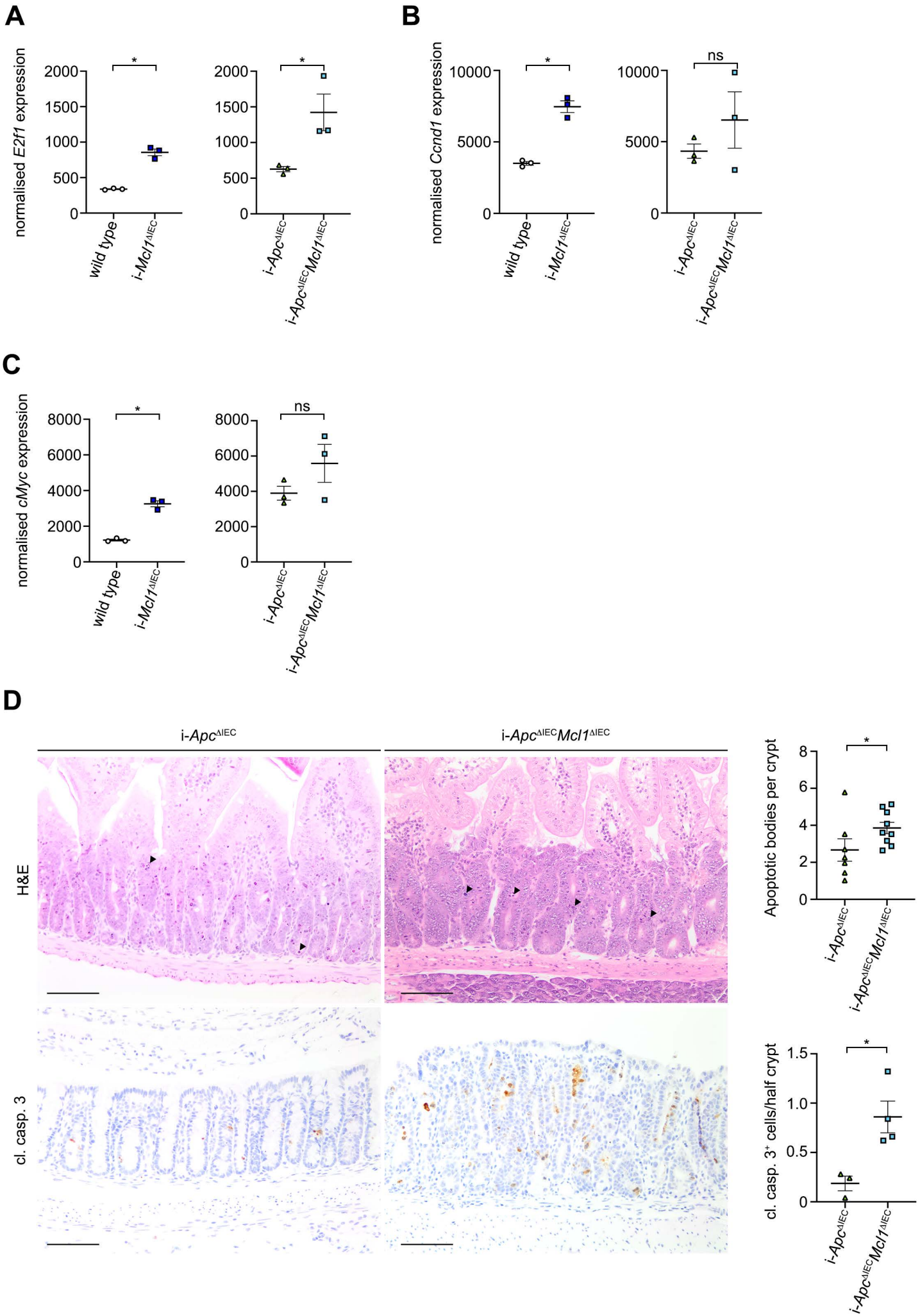

Figure S20. Healy*, Boege*, Hodder* *et. al*

Figure S20: MCL1 is an essential regulator of IEC proliferation. Normalised expression levels of *E2f1* (*A*), *Ccnd1* (*B*) and *cMyc* (*C*) compared between non-recombined wild type controls and i-*Mcl1*$^{\Delta IEC}$ mice as well as i-*Apc*$^{\Delta IEC}$ compared to i-*Apc*$^{\Delta IEC}$*Mcl1*$^{\Delta IEC}$ mice as analysed by RNAseq (n=3 per group). (*D*) Representative H&E images showing apoptotic bodies (upper panel) and cleaved caspsase 3 staining (lower panel) of i-*Apc*$^{\Delta IEC}$ mice compared to age-matched i-*Apc*$^{\Delta IEC}$*Mcl1*$^{\Delta IEC}$ mice. Results from the quantification of apoptotic bodies (top graph) in i-*Apc*$^{\Delta IEC}$ mice (n=7) versus i-*Apc*$^{\Delta IEC}$*Mcl1*$^{\Delta IEC}$ mice (n=9) as well as cleaved caspase 3 positive IEC (bottom graph) in i-*Apc*$^{\Delta IEC}$ mice (n=3) versus i-*Apc*$^{\Delta IEC}$*Mcl1*$^{\Delta IEC}$ mice (n=4) are also shown (scale bars: 100μm). Statistical analysis was conducted by Mann-Whitney test (*A*-*D*) where * $p \leq 0.05$.

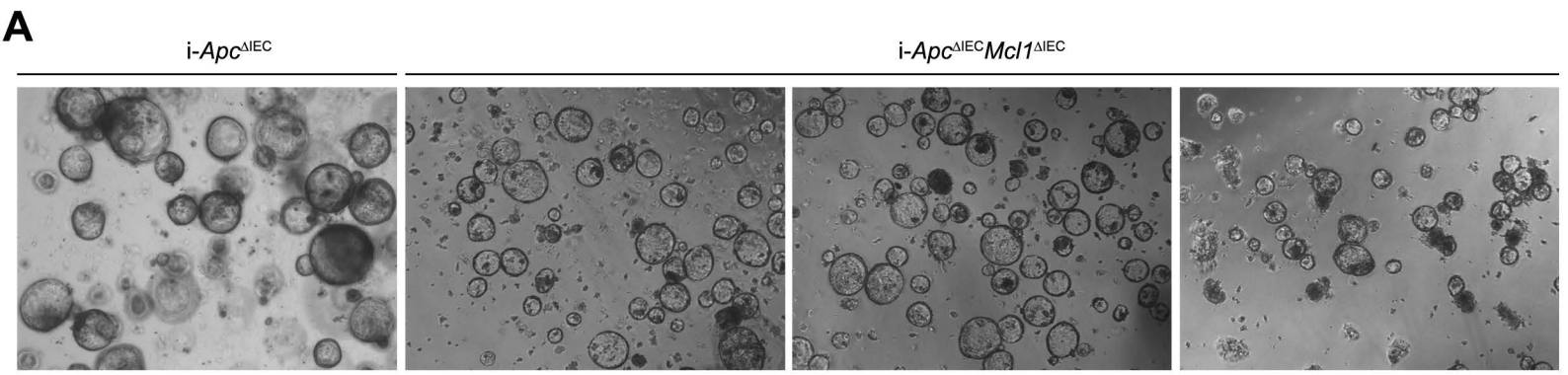

Figure S21. Healy*, Boege*, Hodder* *et. al*

Figure S21: Carcinoma development in *Mcl1*$^{\Delta IEC}$ mice follows the Vogelstein model of colorectal cancer development. (*A*) Representative images of small intestine derived organoids from i-*Apc*$^{\Delta IEC}$ mice or i-*Apc*$^{\Delta IEC}$Mcl1$^{\Delta IEC}$ mice (40x) in vitro (≥5 passages).

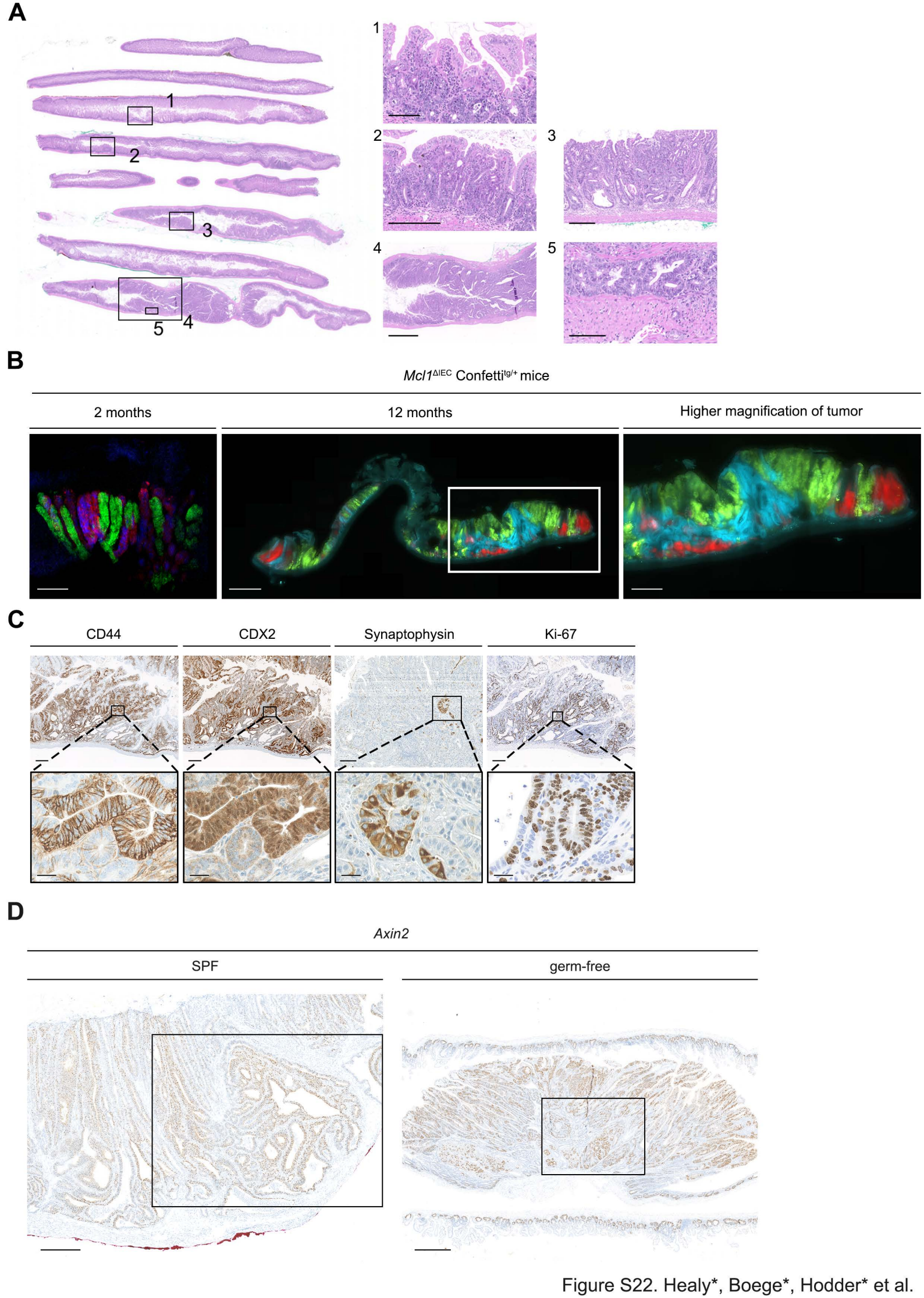

Figure S22. Healy*, Boege*, Hodder* et al.

Figure S22: Carcinoma development in *Mcl1*$^{\Delta IEC}$ mice follows the Vogelstein model of colorectal cancer development. (*A*) Examples of MCL1 deficient tumor qualities used to determine tumor classification in 12-month-old *Mcl1*$^{\Delta IEC}$ mice (Fig. 7*B*). Image 1 illustrates hyperplasia within intestinal crypt cells (scale bar: 100μm), 2 illustrates representative low grade adenoma (LGA) (scale bar: 250μm), 3 illustrates representative high grade adenoma (HGA) (scale bar: 250μm) while images 4 and 5 illustrate representative carcinoma under low (scale bar: 1mm) and high (scale bar: 100μm) magnification. (*B*) Tumor heterogeneity illustrated by representative images of tumors observed in 12-month-old *Mcl1*$^{\Delta IEC}$ Confetti$^{tg/wt}$ mouse (scale bars: 100μm-left, 250μm-centre and 100μm-right). (*C*) Heterogeneous differentiation within carcinoma showing CD44, CDX2, synaptophysin and Ki-67 (scale bars 250μm for upper panel images, 50μm for lower panel images). (*D*) Strong *Axin2* expression in tumors isolated from 12-month-old *Mcl1*$^{\Delta IEC}$ mouse irrespective of whether mice were housed under spf or germ-free conditions determined using *in situ* hybridization (scale bars: 250μm-left, 500μm-right). Areas marked with black boxes represent the areas shown under higher magnification in Figure 7*E*.

A

Gene	Chr:Pos	REF	ALT	Codon variant	Functional Variant	Mucosa, wt	Hyperplasia/ LGD 1 spf	Hyperplasia/ LGD 2 gf	Carcinoma 1 spf	Carcinoma 2 spf	Carcinoma 3 spf	Carcinoma 4 gf	Carcinoma 5 gf
Apc	chr18:34312747	C	T	c.2695C>T	p.Gln899*	./.	./.	./.	./.	C/T (38,41)	./.	./.	./.
Apc	chr18:34316309	A	G	c.6257A>G	p.Asp2086Gly	A/G (50,52)	A/G (32,20)	A/G (27,23)	./.	./.	A/G (37,32)	./.	A/G (22,18)
Lrp5	chr19:3659357	C	T	c.372G>A	p.Thr124Thr	./.	C/T (19,21)	./.	./.	./.	C/T (29,14)	./.	./.
Fbxw7	chr3:84903756	A	G	c.187A>G	p.Asn63Asp	./.	./.	G/G (1,19)	./.	./.	./.	./.	./.
Fbxw7	chr3:84903911	A	G	c.342A>G	p.Glu114Glu	./.	./.	./.	./.	G/G (1,22)	./.	G/G (1,33)	./.
Fbxw7	chr3:84954904	A	G	c.540A>G	p.Glu180Glu	./.	./.	./.	./.	./.	./.	G/G (2,75)	./.
Pole	chr5:110299343	A	C	c.2081A>C	p.Lys694Thr	./.	./.	./.	A/C (18,10)	./.	./.	./.	./.
Arid1a	chr4:133689170	ATATAC	A	c.3289_3293delTATAC	p.Gln1096fs	./.	./.	./.	./.	./.	ATATAC/A (62/24)	./.	./.
Ctnnb1	chr9:120950606	C	A	c.98C>A	p.Ser33Tyr	./.	./.	./.	./.	./.	C/A (23,5)	./.	./.
Ctnnb1	chr9:120950630	C	T	c.122C>T	p.Thr41Ile	./.	./.	C/T (23,14)	C/T (12,6)	./.	./.	./.	./.
Ctnnb1	chr9:120950642	C	T	c.134C>T	p.Ser45Phe	./.	./.	./.	./.	./.	./.	./.	C/T (11,6)

	pathogenic
	potentially pathogenic
	functionally irrelevant
	wild type

Figure S23. Healy*, Boege*, Hodder* et al.

Figure S23: MCL1-deficiency associated carcinoma show a number of pathogenic mutations in key WNT signalling regulating genes. (*A*) Selected mutations detected by whole-exome sequencing and variant filtration. Missense mutations in the genes of interest are displayed by allelic state. The coverage of the position for each allele is given in brackets."./." is the wild type sequence. Exome data were aligned to the Mus musculus reference genome (GRCm38/mm10) and codon variants are displayed according to the following transcript references: Apc - ENSMUST00000079362, Lrp5 - ENSMUST00000176867, Fbxw7 - ENSMUST00000107678, Pole - ENSMUST00000007296, Arid1a - ENSMUST00000105897, Ctnnb1 - ENSMUST00000145093. Abbreviations: Chr:Pos = Position in reference genome; REF = reference allele; ALT = alternative allele; LGD = low grade dysplasia. The color code illustrates the clinical significance of the homolog mutation in humans (see Supplementary Tables S7 – S12 for more information).

Supplemental Information:

Mice

Housing and experimental procedures of all animals were performed in accordance with the Cantonal Veterinary Office (Zurich, Switzerland) under the license numbers ZH217/12 and ZH166/15 or the UK Home Office regulations (licence 70/8646) as well adhering to ARRIVE guidelines. Animals were maintained under specific pathogen free (SPF) conditions at the University of Zurich, Switzerland, or at the CRUK Beatson Institute, Glasgow, Scotland. Germ-free housing of mice was performed within the Clean Mouse Facility of the University of Bern via embryo transfer [1].

Mice with an IEC specific deletion of *Mcl1*, *Mcl1*$^{flx/flx}$ mice [2, 3] were crossed with mice expressing Cre-recombinase under the enterocyte-specific villin promoter, to generate IEC-specific *Mcl1* knockout mice (*Mcl1*$^{flox/flox}$ *Vil1*cre$^{tg/+}$) (*Mcl1*$^{\Delta IEC}$ mice). *Mcl1*$^{\Delta IEC}$ mice were backcrossed onto the *Rag1*$^{-/-}$ background (Jackson Laboratories, mouse strain 002216) to generate *Mcl1*$^{\Delta IEC}$*Rag1*$^{-/-}$ mice. Confetti$^{tg/+}$ mice (Jackson Laboratories, mouse strain 017492 were intercrossed to *Mcl1*$^{\Delta IEC}$ mice to generate *Mcl1*$^{\Delta IEC}$Confetti$^{tg/+}$ mice. These mouse lines were generated at the University of Zurich. Both male and female mice were used for each experiment. Age-matched and littermate mice that did not carry the Villin-Cre transgene were used as wild type control mice.

Mice with an IEC-specific inducible deletion of *Mcl1* (i-*Mcl1*$^{\Delta IEC}$ mice), *Ctnnb1* (i-*Ctnnb1*$^{\Delta IEC}$ mice), *Apc* (i-*Apc*$^{\Delta IEC}$ mice) as well as double knockout mice (i-*Ctnnb1*$^{\Delta IEC}$*Mcl1*$^{\Delta IEC}$ mice and i-*Apc*$^{\Delta IEC}$*Mcl1*$^{\Delta IEC}$ mice) were generated at the CRUK Beatson Institute, Glasgow. Genetic depletion in these mice was typically induced between 6 and 12 weeks of age when weighing over 20g. Genetic alleles used were: *Vil-Cre-ER*^{T2} [4], *Mcl1*^{fl} [5], *Ctnnb1*^{fl} [6] and *Apc*[7]. Recombination was induced using a single intra-peritoneal (IP) injection of 2mg tamoxifen for two consecutive days. A brief overview of each mouse line can be found in Table S1.

Table S1. Description of mouse strains

Mouse strain	Genotype	Housing Location	Description
wild type	Mcl1$^{fl/fl}$ *Vil1*-cre$^{wt/wt}$	University of Zurich University of Bern (Germ Free)	Both *Mcl1* alleles are floxed but mice are Cre negative. No recombination of *Mcl1*.
Mcl1$^{fl/wt}$cre$^{Tg/+}$	*Mcl1*$^{fl/}$wt *Vil1*-cre$^{tg/wt}$	University of Zurich	One floxed *Mcl1* allele and one wild type allele. Mice retain one wild type copy of *Mcl1*.
Mcl1$^{\Delta IEC}$	Mcl1$^{fl/fl}$ *Vil1*-cre$^{tg/wt}$	University of Zurich University of Bern (Germ Free)	Intestinal Epithelial Cell (IEC) specific deletion of *Mcl1*
Rag1$^{-/-}$	*Rag1*$^{-/-}$	University of Zurich	Immune deficient (lack conventional B and T cells)
Mcl1$^{\Delta IEC}$ *Rag1*$^{-/-}$	Mcl1$^{fl/fl}$ *Vil1*-cre$^{tg/wt}$ *Rag1*$^{-/-}$	University of Zurich	Immune deficient (lack conventional B and T cells) IEC specific deletion of *Mcl1*
i-*Mcl1*$^{\Delta IEC}$	*Mcl1*$^{fl/fl}$ *Vil1*-cre-ER^{T2}	CRUK Beatson Institute	Tamoxifen inducible IEC specific deletion of *Mcl1*
i-*Apc*$^{\Delta IEC}$	*Apc*$^{fl/fl}$ *Vil1*-cre-ER^{T2}	CRUK Beatson Institute	Tamoxifen inducible IEC specific deletion of *Apc*
i-*Ctnnb1*$^{\Delta IEC/wt}$	*Ctnnb1*$^{fl/wt}$ *Vil1*-Cre-ER^{T2}	CRUK Beatson Institute	Tamoxifen inducible IEC specific deletion of one copy *Ctnnb1*
i-*Ctnnb1*$^{\Delta IEC/wt}$*Mcl1*$^{\Delta IEC}$	*Ctnnb1*$^{fl/wt}$ *Vil1*-Cre-ER^{T2} *Mcl1*$^{fl/fl}$ *Vil1*-Cre-ER^{T2}	CRUK Beatson Institute	Tamoxifen inducible IEC specific co-deletion of *Mcl1* and one copy of *Ctnnb1*
i-*Apc*$^{\Delta IEC}$*Mcl1*$^{\Delta IEC}$	*Apc*$^{fl/fl}$ *Vil1*-Cre-ER^{T2} *Mcl1*$^{fl/fl}$ *Vil1*-Cre-ER^{T2}	CRUK Beatson Institute	Tamoxifen inducible IEC specific co-deletion of *Mcl1* and *Apc*
Mcl1$^{\Delta IEC}$ Confetti$^{tg/+}$	Mcl1$^{fl/fl}$ *Vil1*-cre$^{tg/wt}$ Confetti Cre$^{tg/wt}$	University of Zurich	Genetic IEC specific co-deletion of *Mcl1* and expression of Confetti

In situ Hybridization

RNA ISH was performed on FFPE tissues according to the manufacturer`s protocol using five commercially available probes. 1) A probe designated Mm-Mcl1 (by Advanced Cell Diagnostics (ACD); ACD catalog number #317241), and targeting nucleotides 495-1678 of murine Mcl1 gene. 2) A probe designated Mm-Lgr5 (by Advanced Cell Diagnostics (ACD); ACD catalog number #312171), and targeting nucleotides 2165-3082 of murine Lgr5 gene. 3) A probe designated Mm-Olfm4 (by Advanced Cell Diagnostics (ACD); ACD catalog number #311838), and targeting nucleotides 25-1043 of murine Olfm4 gene. 4) A probe designated Hs-MCL1 (by Advanced Cell Diagnostics (ACD); ACD catalog number #588851), and targeting nucleotides 1514-3532 of human Mcl1 gene. 5) A probe designated Hs-OLFM4 (by Advanced Cell Diagnostics (ACD); ACD catalog number #311048) targeting nucleotides 1111-2222 of human OLFM4 gene.

Bacterial DNA isolation

Bacterial DNA was isolated from stool samples that were previously stored at -80°C. DNA was isolated using the PureLink Microbiome DNA purification kit (Invitrogen, A29789) according to the manufacturer's protocols.

PCR for bacterial DNA

The 16S PCR was performed as described previously[8] with some modifications. Reactions were performed in a final volume of 50 μl containing 10 ng of fecal DNA template[9], 200 nM dNTP, 200 nM of each primer, 1 U HotStarTaq polymerase (Qiagen), and 1-fold CoralLoad PCR Buffer (Qiagen). "Universal" primers were used to amplify the genes encoding 16S rRNA from all bacterial groups: Forward primer (5′- ACTCCTACGGGAGGCAGCAGT -3′) and reverse primer, (5′- ATTACCGCGGCTGCTGGC -3′)[8], resulting in an 197 bp amplikon. PCR assays were performed in a C1000 Touch Thermal Cycler (Biorad) using the following

program: 95°C for 5 min, then 25 cycles of 94°C for 60 sec, 55°C for 90 sec and 72°C for 60 sec. These cycles were followed by 72°C for 10 minutes, and storage at 4°C. Amplified products were separated on a 2% (m/v) agarose (Invitrogen) gel in Tris/acetate/EDTA buffer (National diagnostics) containing 1-fold GelRed Nucleic Acid Gel Stain (Biotium).

FISH for Bacterial 16s rRNA

5μm tissue sections of paraffin-fixed colon samples were deparaffinated in xylol to ethanol baths in decreasing ratios. Tissue sections were permeabilized in hybridization buffer containing PBS 0.9M NaCl, 20mM Tris-HCl, and 0.1% sodium dodecyl sulfate for 10 mins at 50°C. Hybridization was performed with an Alexafluor-647 labeled universal 16s rRNA bacterial probe (5'-[AF 647] GCTGCCTCCCGTAGGAGT-3'; Eurofin genomics, 10nM per section) diluted in hybridization buffer for 4 hours at 50°C, followed by two washing steps using the PBS 0.9M NaCl and 20mM Tris-HCl. DAPI was applied diluted in the washing buffer for 5 mins at RT, followed by one washing step. Samples were mounted with Vectashield (Vector laboratories) and stored in the dark at 4°C. Images were recorded with an LCI laser scanning confocal microscope (Zeiss) or a pannoramic 250 flash II scanner (3DHISTECH).

Western blot

Colon tissue was isolated from 2-month-old mice immediately after euthanasia and placed in ice-cold PBS containing phosphatase inhibitor cocktail tablets (PhosStop, Roche #04906837001) and protease inhibitor cocktail tablets (cOmplete EDTA-free tabs, Roche #11873580001). Intestinal tissue was opened longitudinally and the epithelial layer was scraped directly into 200µl of ice-cold complete RIPA lysis buffer. All antibodies used for western blot analysis can be found in Table S2. Samples were run on 4-20% Mini-PROTEAN® TGX Stain-Free™ gels (Bio-Rad Laboratories, #456-8093) and were developed using a ChemiDoc™ XRS+ imaging machine (Bio-Rad Laboratories) with Image Lab™ software.

Organoid Isolation and Culturing

In brief, small intestinal tissue was dissected, flushed with PBS and opened longitudinally, with villi and mucous layers then removed mechanically by scraping. The resulting intestinal samples were washed with PBS, incubated with 2mM EDTA at 4°C for 30 minutes followed by further washing and filtration through a 70μm mesh in order to isolate intestinal crypts. These isolated crypts were suspended in growth factor reduced Matrigel® (Corning), plated in 10-20μl droplets, and incubated at 37°C in 5% CO2. i-*Apc*$^{\Delta IEC}$ or i-*Apc*$^{\Delta IEC}$*Mcl1*$^{\Delta IEC}$ organoids were maintained in Advanced DMEM/F12 growth media (Thermo), supplemented with 2mM L-glutamine, 10mM HEPES, 12.5% (w/v) BSA, 100ng/ml murine NOGGIN, 50ng/ml murine EGF, and 1 x proprietary B27 and N2 supplements (Thermo). Wild type control or i-*Mcl1*$^{\Delta IEC}$ organoids were maintained in the same media, supplemented with 0.5μg/ml murine R-SPONDIN1.

636 **Table S2. Table of antibodies**

Antibody Name	Company	Catalogue Nmber
Anti-CD90 / Thy1 antibody (IBL-6/23)	Abcam	Cat# ab3105; RRID: AB_2287350
Anti-MLKL (phospho S345) antibody	Abcam	Cat# ab196436; RRID: AB_2687465
CDX2 antibody (EPR2764Y) (IHC)	Abcam	Cat# ab76541; RRID: AB_1523334
Synaptophysin antibody (YE269) (IHC)	Abcam	Cat# ab32127; RRID: AB_2286949
BrdU antibody (IHC)	BD Biosciences	Cat# 347580; RRID: AB_400326
CD45R/B220 antibody (IHC)	Becton Dickinson	Cat# 553084; RRID: AB_394614
Rat Anti-Mouse F4 / 80 (Macrophages) Monoclonal Antibody (IHC)	BMA Biomedicals	Cat# T-2006; RRID: AB_1227368
BAK Antibody	Cell Signaling Technology	Cat# 3814S; RRID: AB_2290287
BAX Antibody	Cell Signaling Technology	Cat# 2772S; RRID: AB_10695870
BCL2 Antibody	Cell Signaling Technology	Cat# 2876S; RRID: AB_2064177
BCL-xL Antibody	Cell Signaling Technology	Cat# 2762S; RRID: AB_329920
BID Antibody (Mouse Specific)	Cell Signaling Technology	Cat# 2003S; RRID: AB_10694562
BIM (C34C5) Rabbit mAb	Cell Signaling Technology	Cat# 2933S; RRID: AB_1030947
Caspase-8 Antibody (Mouse Specific)	Cell Signaling Technology	Cat# 4927S; RRID: AB_10694563
Caspase-9 (C9) Mouse mAb	Cell Signaling Technology	Cat# 9508S; RRID: AB_2068620
Cleaved Caspase-3 (Asp175) (5A1E) Rabbit mAb	Cell Signaling Technology	Cat# 9664P; RRID: AB_2070042
Cleaved Caspase-3 (Asp175) Antibody (IHC)	Cell Signaling Technology	Cat# 9661; RRID: AB_2341188
GAPDH (D16H11) XP Rabbit mAb antibody	Cell Signaling Technology	Cat# 5174S; RRID: AB_10622025
MCL1 (D35A5) Rabbit mAb	Cell Signaling Technology	Cat# 5453P; RRID: AB_10828726
Olfm4 (D6Y5A) Rabbit mAb (Mouse Specific) (IHC)	Cell Signaling Technology	Cat# 9718S; RRID: AB_2118009
Pan-Keratin (C11) Mouse mAb	Cell Signaling Technology	Cat# 4545S; RRID: AB_490860
PCNA (PC10) Mouse mAb	Cell Signaling Technology	Cat# 2586S; RRID: AB_2160343
Rabbit Anti-beta-Catenin Monoclonal Antibody (IHC)	Cell Signaling Technology	Cat# 9582S; RRID: AB_823447
Polyclonal Rabbit Anti-Cytokeratin (IHC)	DAKO	Cat# Z0622; RRID: AB_2650434
Polyclonal Rabbit Anti Human Lysozyme EC 3.2.1.17 antibody (IHC)	DAKO	Cat# A0099; RRID: AB_2341230
SOX9 (EP317) Rabbit Monoclonal Antibody	Epitomics	Cat# AC-0284RUO
Rabbit Anti-Human CD3 Monoclonal Antibody, Unconjugated, Clone SP7 (IHC)	Lab Vision	Cat# RM-9107-S; AB_149922
Rabbit Anti-Human Ki67 (Ki-67) Monoclonal Antibody, Unconjugated, Clone SP6 (IHC)	Lab Vision	Cat# RM-9106-S; RRID: AB_149707

Rabbit Anti-Gamma H2AX, phospho (Ser139) Polyclonal Antibody (IHC)	Novus Biologicals	Cat# NB100-384; RRID: AB_350295
Rabbit Anti-MCL1 Antibody	Rockland	Cat# 600-401-394; RRID: AB_2266446
CD44 (HCAM) (IM7) Antibody (IHC)	Santa Cruz Biotechnology	Cat# sc-18849; RRID: AB_2074688
MLKL Antibody (Y-14)	Santa Cruz Biotechnology	Cat# sc-165025; RRID: AB_10839183
Anti-α-Tubulin antibody, Mouse monoclonal	Sigma-Aldrich	Cat# T8203-25UL; RRID: AB_1841230
Mouse Anti-Actin, alpha-Smooth Muscle Monoclonal Antibody (IHC)	Sigma-Aldrich	Cat# A2547; RRID: AB_476701

Histological Scoring

Histological scoring was performed by a pathologist in a blinded fashion by analysing H&E stained slides from 2-month-old wild type control, *Mcl1*$^{\Delta IEC}$, *Rag1*$^{-/-}$ or *Mcl1*$^{\Delta IEC}$*Rag1*$^{-/-}$ mice. Histological scores were attributed independently to the small intestine and colon of each mouse. Histological scoring was based on architectural changes (crypt hyperplasia and villin/crypt ratio length), inflammatory changes (neutrophil and lymphoplasmocyte infiltration), epithelial damage (epithelial surface damage) and cell death (apoptosis) using a modified established scoring system [10] designed to discriminate between normal tissue (score = 0) and mild (score = 1), moderate (score = 2) or severe (score = 3) pathology. Detailed criteria for each category are provided in Table S3 and representative images of each scoring criteria are displayed as Supplementary Data 1. Histological score was determined using 5 mice per group.

678 **Table S3. Histological scoring criteria**

	Normal (score = 0)	Mild (score = 1)	Moderate (score = 2)	Severe (score = 3)
Architectural changes:				
Crypt hyperplasia	Parallel crypts separated with stroma	Increased amount, decreased diameter, elongation irregular shape of the crypts, enlarged epithelial cells	Increased amount, decreased diameter, elongation irregular shape of the crypts, crypts located “back to back”, branched crypts, enlarged epithelial cells OR multi-layered epithelium in the crypts	Increased amount, decreased diameter, elongation irregular shape of the crypts, crypts located “back to back”, branched crypts, enlarged epithelial cells AND multi-layered epithelium in the crypts
Villli/crypt length ratio (small intestine only)	Between 3:1 and 5:1	Approximately 2:1	Approximately 1:1	Blunted or flat villi
Inflammatory changes:				
Neutrophils	0-3 cells per high power field	5-10 cells per high power field	>10 cells per high power field	Abscess
Lymphoplasmocytes	1 lymphocyte per 4-5 epithelial cells within the crypt. discrete lympho-plasmocytes in lamina propria, isolated lymphoid follicles	Mildly increased amount of inflammatory cells in the epithelium or lamina propria,	Lamina propria expansion by a mixed inflammatory infiltrate, increased amount of lymphoid follicles	Lamina propria expansion by a mixed inflammatory infiltrate, AND multiple or large reactive lymphoid follicles
Epithelial damage				
Superficial damage	Normal epithelium	Changes in cytoplasm and nuclei (accumulation and vacuolization), goblet cells reduction	Changes in cytoplasm and nuclei (accumulation and vacuolization), goblet cells reduction AND isolated erosions	Changes in cytoplasm and nuclei (accumulation and vacuolization), goblet cells reduction AND multiple erosions or ulceration
Apoptosis	No apoptosis	Numerous apoptotic bodies in the crypt epithelium	Apoptotic bodies in the crypt’s lumen	Dilated crypts with flattened epithelium (cystic dilated crypts)

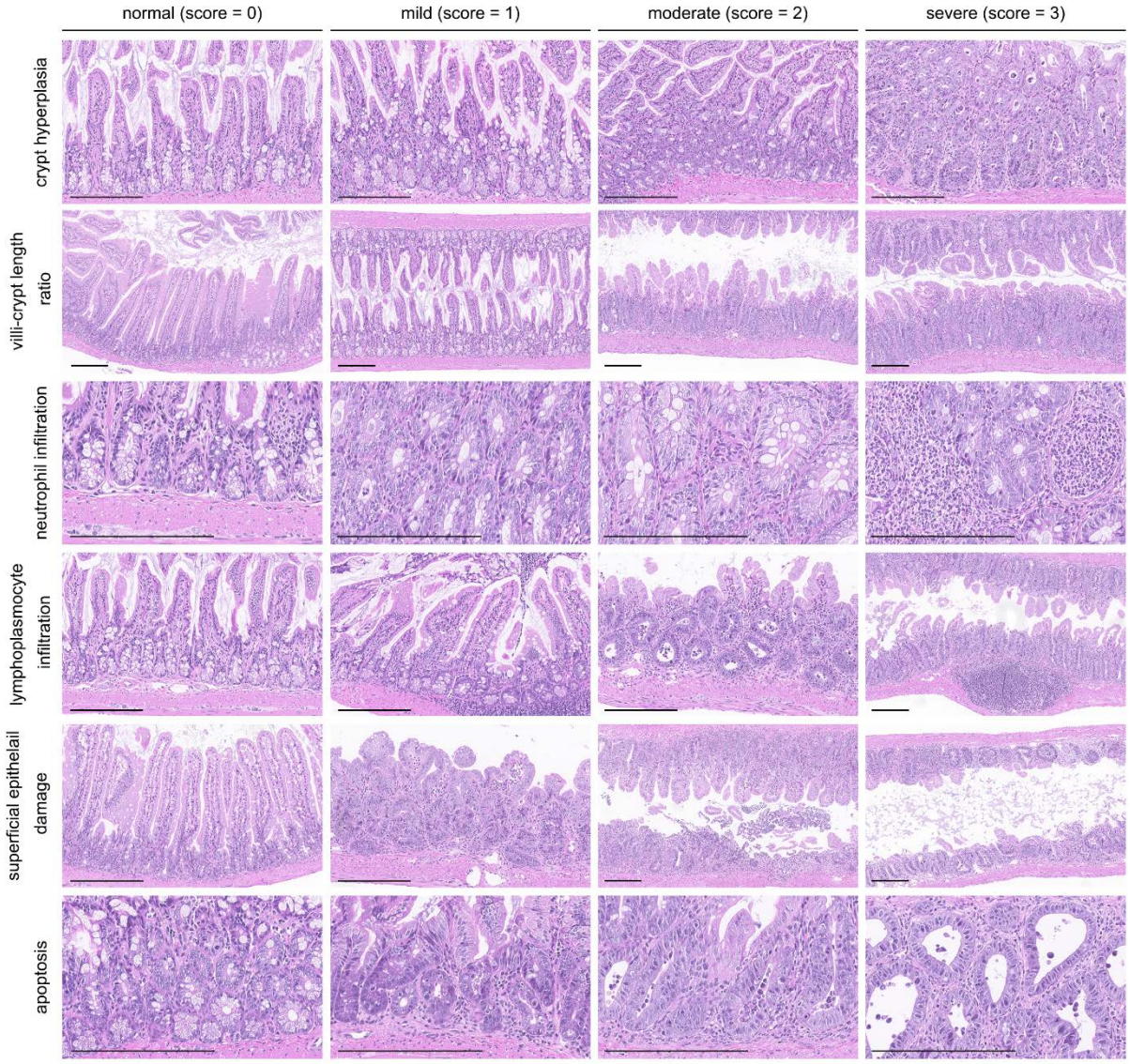

679

680 **Supplementary Data 1.** Representative H&E images of small intestine which illustrate the
681 criteria needed to be considered wild type (score = 0), mild (score = 1), moderate (score = 2)
682 or severe (score = 3) in relation to crypt hyperplasia, neutrophil or lymphoplasmocyte
683 infiltration, epithelial damage, villi-crypt length ratio and apoptosis during histological scoring
684 (200μm scale bar).

685

686

687

688

Sanger Sequencing and Whole Exome Sequencing

Genomic DNA was isolated from FFPE tissue blocks using Machery & Nagel's NucleoSpin FFPE Kit and analysed by either Sanger Sequencing or Whole Exome Sequencing. For both, regions of normal tissue, hyperplasia, low-grade hyperplasia, high-grade hyperplasia or carcinoma were identified based on previously described criteria [11]. For Sanger Sequencing, AmpliTaq Gold polymerase was used to amplify 296bp of the *Ctnnb*1 gene (exon 2) following the manufacturer's recommendations (Primer sequences obtained from Huang et al. [12] fwd: 5'- TACAGGTAGCATTTTCAGTTC AC -3'; rev: 5'- TAGCTTCCAAACACAAATGC -3'). PCR products were sequenced at Microsynth, Balgach, Switzerland. Sequences were aligned against the reference NC_000075.6 (chr9:120950522-120950749 *Mus musculus* strain C57BL/6J). Codon changes were outlined according to transcript reference NM_000076.5.

For array Comparative Genomic Hybridization (aCGH) and Synteny analysis, regions of healthy tissue, hyperplasia or carcinoma were identified based on previously described criteria [11]. Genomic DNA was isolated from FFPE tissue blocks using Macherey & Nagel's NucleoSpin FFPE Kit before aCGH and Synteny analysis were performed as previously described [13].

Whole exome sequencing of tumor and non-tumor tissue was performed on genomic DNA isolated from formalin-fixed paraffin-embedded (FFPE) samples at Ontogenetic Corporations, Atlanta (GA, USA). Samples were chosen according to previously published criteria [11, 14] to distinguish between normal tissue, hyperplastic tissue, low grade adenoma, high grade adenoma and carcinoma. Tissue samples matching these criteria were punched out of the FFPE blocks and genomic DNA was extracted with the NucleoSpin FFPE kit (Macherey & Nagel). Sequencing data have been deposited at the European Nucleotide Archive under the accession number PRJEB20295.

Enrichment of the whole exome (Agilent SureSelect Mouse All Exon kit) and subsequent Illumina sequencing on a HighSeq2500 (125bp PE) was performed at Ontogenetic Corporations, Atlanta (GA, USA). Ontogenetic Corporations processed the sequence reads on the DNAnexus platform (Mountain View, CA, USA) using the advanced mouse exome analysis

pipeline. Quality filtered reads were aligned against the mouse reference genome (GRCm38/mm10) using BWA[15]. After removing PCR duplicates (PicardTools: Mark duplicates (Broad Institute)) GATK's Unified Genotyper was used to call variants after realignment and base quality score recalibration [16].

Raw variants were filtered based on GATK's recommendations. Variants were divided into SNPs and INDELs to apply different parameters during the filtration step. For retaining SNPs in the dataset the criteria were "QD > 2.0 & FS < 60.0 & MQ > 40.0 & MQRankSum > -12.5 & ReadPosRankSum > -8.0". The selected INDELs have to fulfill "QD > 2.0 & FS < 200.0 & ReadPosRankSum > -20.0" to be selected. Afterwards the SNP and INDEL dataset per sample was combined and variant filtration steps for depth and genotype quality can be applied (DP>=10; QUAL>=30). Variants were annotated and functional effects were predicted with SNPEff [17]. The exome datasets were filtered for the WNT, TGF-β, PI3K, RTK-RAS and P53 signaling pathways. A full list of target genes can be found in Table S4 to S9.

An exome coverage of 38.93x – 124.87x was achieved containing ~ 9000 – 15000 filtered variants (see Table S7). This low level of variance in the whole exome was unsurprising, since the strain used in this mouse model is of a pure inbred background (C57BL/6), as was used to prepare the *Mus musculus* reference genome (for detailed information and discussion see Fairfield 2015) [18].

Table S4. Results after SNP calling by GATK's Unified Genotyper.

Sample	*coverage (exome)*	*Variants*	*n SNPs*	*n Insertions*	*n Deletions*	*n Complex*
Carcinoma 1 spf	48.72x	20337	18100	526	1690	21
Carcinoma 2 spf	82.52x	25047	22023	629	2361	34
Carcinoma 4 gf	109.09x	28720	24509	1080	3053	78
Mucosa, wt	124.87x	18491	15245	600	2615	31
Hyperplasia/LGD 1 spf	66.87x	19465	16769	621	2045	30
Carcinoma 3 spf	78.45x	21328	18284	694	2321	29
Carcinoma 5 gf	38.93x	18920	16627	629	1647	17
Hyperplasia/LGD 2 gf	70.18x	24584	21150	842	2543	49

737 **Table S5.** Variant statistics after individual filtration of SNPs and INDELs (parameters are
738 mentioned in the text).

Sample	*coverage (exome)*	*Variants*	*n SNPs*	*n Insertions*	*n Deletions*	*n Complex*
Carcinoma 1 spf	48.72x	11034	9319	338	1359	18
Carcinoma 2 spf	82.52x	13334	10998	397	1913	26
Carcinoma 4 gf	109.09x	15429	12308	677	2382	62
Mucosa, wt	124.87x	11388	8679	454	2233	22
Hyperplasia/LGD 1 spf	66.87x	12576	10329	474	1746	27
Carcinoma 3 spf	78.45x	13730	11200	530	1975	25
Carcinoma 5 gf	38.93x	9189	7600	337	1238	14
Hyperplasia/LGD 2 gf	70.18x	12457	9966	506	1950	35

739

740 **Table S6.** Variants after applying the filters for depth and genotype quality (DP
741 >=10,QUAL>=30).

Sample	*coverage (exome)*	*Variants*	*n SNPs*	*n Insertions*	*n Deletions*	*n Complex*
Carcinoma 1 spf	48.72x	9199	7532	323	1326	18
Carcinoma 2 spf	82.52x	11332	9047	380	1879	26
Carcinoma 4 gf	109.09x	13651	10578	667	2344	62
Mucosa, wt	124.87x	10136	7457	445	2212	22
Hyperplasia/LGD 1 spf	66.87x	10992	8800	458	1707	27
Carcinoma 3 spf	78.45x	12042	9554	515	1948	25
Carcinoma 5 gf	38.93x	7949	6406	323	1206	14
Hyperplasia/LGD 2 gf	70.18x	11057	8617	489	1916	35

742

743 **Table S7.** Genes of interest from the signaling pathways of WNT, TGF-beta, RTK-RAS and

744 p53.

Chr	Start	End	Gene	Length	Strand	Name
				WNT signalling pathway		
19	30545863	30549665	*Dkk1*	3802	-	dickkopf WNT signaling pathway inhibitor 1
3	132085292	132180304	*Dkk2*	95012	-	dickkopf WNT signaling pathway inhibitor 2
7	112116017	112159057	*Dkk3*	43040	-	dickkopf WNT signaling pathway inhibitor 3
8	22624043	22627547	*Dkk4*	3504	+	dickkopf WNT signaling pathway inhibitor 4
19	3584828	3686564	*Lrp5*	101736	-	low density lipoprotein receptor-related protein 5
6	134446476	134566965	*Lrp6*	120489	-	low density lipoprotein receptor-related protein 6
5	128600844	128604093	*Fzd10*	3249		frizzled class receptor 10
X	95420318	95444872	*Amer1*	24554	-	*APC* membrane recruitment 1 (Fam123b)
11	108920349	108950783	*Axin2*	30434	+	axin 2
18	34220924	34318608	*Apc*	97684	+	adenomatosis polyposis coli
9	120929216	120960507	*Ctnnb1*	31291	+	catenin (cadherin associated protein), beta 1
19	55741820	55933654	*Tcf7l2*	191834	+	transcription factor 7 like 2, T cell specific, HMG box
3	84815268	84979198	*Fbxw7*	163930	+	F-box and WD-40 domain protein 7
4	133679008	133756769	*Arid1a*	77761	-	AT-rich interactive domain-containing protein 1A
11	52252371	52283014	*Tcf*	30643	-	transcription factor 7, T cell specific
15	61985391	61990374	*Myc*	4983	+	myelocytomatosis oncogene
3	131110471	131224356	*Lef1*	113885		lymphoid enhancer binding factor 1
5	144767732	144859778	*Trrap*	92046	+	transformation/transcription domain-associated protein
6	72626378	72789254	*Tcf7l1*	162876	-	transcription factor 7 like 1 (T cell specific, HMG box)
				TGF-beta signalling		
4	47353222	47414931	*Tgfbr1*	61709	+	transforming growth factor, beta receptor I
9	116087698	116175363	*Tgfbr2*	87665	-	transforming growth factor, beta receptor II
2	48814109	48903269	*Acvr2a*	89160	+	activin receptor IIA
15	101174067	101213679	*Acvr1b*	39612	+	activin A receptor, type 1B
18	76241580	76305731	*Smad2*	64151	+	SMAD family member 2
9	63646767	63757994	*Smad3*	111227	-	SMAD family member 3
18	73639009	73703780	*Smad4*	64771	-	SMAD family member 4
				PI3K signalling		
7	142650766	142666816	*Igf2*	16050	+	insulin-like growth factor 2
7	67952827	68233668	*Igf1r*	280841	+	insulin-like growth factor I receptor
8	10984681	11008458	*Irs2*	23777	-	insulin receptor substrate 2
13	101680563	101768217	*Pik3r1*	87654	-	phosphatidylinositol 3-kinase, regulatory subunit, polypeptide 1
3	32397671	32466107	*Pik3ca*	68436	+	phosphatidylinositol 3-kinase, catalytic, alpha polypeptide
19	32757497	32826160	*Pten*	68663	+	phosphatase and tensin homolog
				RTK-RAS signalling		
11	98412470	98437716	*Erbb2*	25246	+	erb-b2 receptor tyrosine kinase 2
10	128567523	128589652	*Erbb3*	22129	-	erb-b2 receptor tyrosine kinase 3
6	145216699	145250239	*Kras*	33540	-	Kirsten rat sarcoma viral oncogene homolog
3	103058285	103067914	*Nras*	9629	+	neuroblastoma ras oncogene
6	39603237	39725463	*Braf*	122226	-	Braf transforming gene
5	142484839	142551098	*Radil*	66259	-	Ras association and DIL domains
				P53 signalling		
11	69580359	69591873	*Trp53*	11514	+	transformation related protein 53
9	53439149	53536740	*Atm*	97591	-	ataxia telangiectasia mutated
				additional genes of interest		
5	116439275	116591817	*Srrm4*	152542	-	serine/arginine repetitive matrix 4
6	39592574	39603382	*Ndufb2*	10808	+	NADH dehydrogenase (ubiquinone) 1 beta subcomplex, 2
6	64729125	64731245	*Atoh1*	2120	+	atonal bHLH transcription factor 1
7	83642825	83745726	*Il16*	102901	-	interleukin 16
9	106892825	107231909	*Dock3*	339084	-	dedicator of cyto-kinesis 3
15	81585351	81652077	*Ep300*	66726	+	E1A binding protein p300
11	112782224	112787760	*Sox9*	5536	+	SRY (sex determining region Y)-box 9
5	110286306	110337474	*Pole*	51168	+	polymerase (DNA directed), epsilon
9	111228228	111271791	*Mlh1*	43563	-	mutL homolog 1
12	85234529	85270591	*Mlh3*	36062	-	mutL homolog 3
17	87672330	87723713	*Msh2*	51383	+	mutS homolog 2
13	92211872	92355003	*Msh3*	143131	-	mutS homolog 3
17	87975050	87990883	*Msh6*	15833	+	mutS homolog 6
5	143909964	143933968	*Pms2*	24004	+	postmeiotic segregation increased 2 (*S. cerevisiae*)

Table S8. Identified variants per sample within the gene regions of interest. Variants were filtered to a depth of 10 and genotype quality of 30.

Gene	Chr:Pos	REF	ALT	Codon variant	Functional Variant	Functional Consequence	Ensembl Transcript	rs ID	Mucosa. wt	Hyperplasia /LGD 1 spf	Hyperplasia /LGD 2 gf	Carcinoma 1 spf	Carcinoma 2 spf	Carcinoma 3 spf	Carcinoma 4 gf	Carcinoma 5 gf
Erbb3	chr10:128570846	T	C	c.3192+90A>G		intron_variant(MODIFIER)		.	./.	./.	./.	0/1:7,3:10	./.	./.	./.	./.
Erbb3	chr10:128571949	T	C	c.2687-158A>G		intron_variant(MODIFIER)			./.	./.	./.	./.	0/1:13,4:17	./.	./.	./.
Erbb3	chr10:128575875	CAT	C	T		intron_variant(MODIFIER)	ENSMUST00000082059	rs228017517	./.	0/1:35,13:49	0/1:18,11:30	0/1:3,10:15	0/1:0,10:58	0/1:26,14:41	0/1:0,11:89	0/1:12,11:24
Erbb3	chr10:128584505	T	A	c.422-69A>T		intron_variant(MODIFIER)		.	./.	./.	./.	./.	./.	./.	./.	0/1:9,4:13
Erbb3	chr10:128584507	C	A	c.422-71G>T		intron_variant(MODIFIER)		.	./.	./.	./.	./.	./.	./.	./.	0/1:10,4:14
Axin2	chr11:108931615	CG	C	c.956+37delG		intron_variant(MODIFIER)	ENSMUST00000052915		0/1:41,16:61	./.	./.	./.	./.	./.	./.	./.
Sox9	chr11:112783794	GC	G	c.432-14delC		intron_variant(MODIFIER	ENSMUST00000000579	rs252793042	0/1:9,6:20	./.	./.	./.	./.	./.	./.	./.
Msh3	chr13:92306459	CT	C	-		downstream_gene_variant(MODIFIER)	ENSMUST00000190462	rs220719938	0/1:0,6:66	0/1:10,17:35	0/1:21,12:45	./.	./.	0/1:18,12:41	0/1:29,28:77	0/1:12,12:31
Ep300	chr15:81623553	AT	A	c.2134+29delT		intron_variant(MODIFIER)	ENSMUST00000068387	rs237317619	./.	./.	0/1:35,21:78	./.	./.	0/1:37,19:82	0/1:42,20:81	./.
Ep300	chr15:81636274	CT	C	c.3725+41delT		intron_variant(MODIFIER)		rs255017404	0/1:0,8:206	./.	0/1:0,11:126	./.	./.	0/1:0,10:155	./.	0/1:39,12:54
Msh2	chr17:87679692	TA	T	c.367-107delA		intron_variant(MODIFIER)	ENSMUST00000024967		0/1:18,29:51	./.	0/1:17,20:40	./.	./.	./.	./.	./.
Apc	chr18:34312747	C	T	c.2695C>T	p.Gln899*	stop_gained(HIGH|NONSENSE	ENSMUST00000079362		./.	./.	./.	./.	0/1:38,41:79	./.	./.	./.
Apc	chr18:34316309	A	G	c.6257A>G	p.Asp2086Gly	missense_variant(MODERATE		rs47505115	0/1:50,52:102	0/1:32,20:52	0/1:27,23:50	./.	./.	0/1:37,32:69	./.	0/1:22,18:40
Lrp5	chr19:3659357	C	T	c.372G>A	p.Thr124Thr	synonymous_variant(LOW|SILENT)	ENSMUST00000176867		./.	0/1:19,21:40	./.	./.	./.	0/1:29,14:43	./.	./.
Acvr2a	chr2:48893385	CT	C	c.817-121delT		intron_variant(MODIFIER)	ENSMUST00000063886	rs233268672	0/1:14,17:42	./.	./.	./.	./.	0/1:17,11:32	0/1:12,13:28	./.
Pik3ca	chr3:32440531	AGT	A	c.1060-95_1060-94delGT		intron_variant(MODIFIER)		rs231243003	./.	./.	0/1:4,6:10	1/1:2,13:15	./.	./.	./.	./.
Pik3ca	chr3:32440553	A	T	c.1060-74A>T		intron_variant(MODIFIER)	ENSMUST00000029201		./.	./.	./.	./.	0/1:31,11:42	./.	./.	./.
Pik3ca	chr3:32449854	CT	C	c.1747-54delT		intron_variant(MODIFIER)		.	./.	./.	0/1:22,9:32	./.	0/1:28,12:45	./.	./.	./.
Fbxw7	chr3:84903756	A	G	c.187A>G	p.Asn63Asp	missense_variant(MODERATE|MSSEN		rs3683473	./.	./.	1/1:1,19:20	./.	./.	./.	./.	./.
Fbxw7	chr3:84903911	A	G	c.342A>G	p.Glu114Glu	synonymous_variant(LOW|SILENT)		rs3684554	./.	./.	./.	./.	1/1:1,22:23	./.	1/1:1,33:34	./.
Fbxw7	chr3:84954904	A	G	c.540A>G	p.Glu180Glu	synonymous_variant(LOW|SILENT)	ENSMUST00000107678	rs30008104	./.	./.	./.	./.	./.	./.	1/1:2,75:77	./.
Fbxw7	chr3:84967383	AT	A,ATT	c.871-56delT		intron_variant(MODIFIER)		rs221049948	0/1:42	0/1:32	0/2:39	0/2:16	./.	./.	0/2:28	0/2:15
Fbxw7	chr3:84977650	GA	G	c.*110delA		3_prime_UTR_variant(MODIFIER		rs238194117	./.	./.	./.	./.	./.	1/1:2,22:33	1/1:3,31:39	1/1:1,12:18
Nras	chr3:103063308	G	GTT	c.451-21_451-20insTT		intron_variant(MODIFIER)	ENSMUST00000029445	rs242625067	./.	./.	./.	./.	./.	0/1:26,16:46	0/1:29,15:58	./.
Lef1	chr3:131189251	GT	G,GTT	c.542-83delT		intron_variant(MODIFIER)	ENSMUST00000098611		0/1:43	./.	0/1:31	0/2:24	./.	./.	0/1:28	./.
Arid1a	chr4:133689170	ATATAC	A	c.3289_3293delTATAC	p.Gln1096fs	frameshift_variant(HIGH)	ENSMUST00000105897	./.	./.	0/1:62,24:88		./.	./.	./.	./.	./.
Pole	chr5:110299354	A	C	c.801+159A>C		intron_variant(MODIFIER)	ENSMUST00000007296	rs263341953	./.	./.	./.	./.	0/1:9,4:13	./.	./.	./.
Pole	chr5:110299343	A	C	c.2081A>C	p.Lys694Thr	missense_variant(MODERATE|MSSEN			./.	./.	./.	0/1:18,10:28	./.	./.	./.	./.
Srrm4	chr5:116449334	TG	T	n.187+9899delG		intron_variant(MODIFIER)	ENSMUST00000126959	rs257407124	./.	./.	./.	./.	./.	0/1:4,6:13	./.	./.
Srrm4	chr5:116467875	GGA	G	-		upstream_gene_variant(MODIFIER			./.	./.	0/1:8,14:52	./.	./.	./.	./.	./.
Radil	chr5:142544859	CAG	C	c.23+32_23+33delCT		intron_variant(MODIFIER)	ENSMUST00000085758		./.	./.	./.	./.	./.	./.	./.	0/1:4,7:11
Trrap	chr5:144780182	C	T	c.450+115C>T		intron_variant(MODIFIER)		-	./.	./.	./.	0/1:23,8:31	./.	./.	./.	./.
Trrap	chr5:144780196	C	T	c.450+129C>T		intron_variant(MODIFIER)	ENSMUST00000038980		./.	./.	./.	0/1:17,6:23	./.	./.	./.	./.
Trrap	chr5:144780210	C	T	c.450+143C>T		intron_variant(MODIFIER)			./.	./.	./.	0/1:12,5:18	./.	./.	./.	./.
Ndufb2	chr6:39596677	AT	A	n.364+83delT		intron_variant(MODIFIER)	ENSMUST00000002490	rs239777375	./.	./.	./.	./.	./.	./.	./.	0/1:9,6:21
Ndufb2	chr6:39598377	GT	GTT,G	n.460+18_460+19insT		intron_variant(MODIFIER)		rs249436801	./.	./.	./.	0/1:56	./.	./.	./.	0/2:42
Braf	chr6:39648311	GAA	G,GA	c.1123+137_1123+138delTT		intron_variant(MODIFIER)	ENSMUST00000101497	rs216953796	./.	./.	0/2:33	./.	./.	0/2:31	0/1:46	./.
Braf	chr6:39648327	G	A	c.1123+123C>T		intron_variant(MODIFIER)			./.	./.	0/1:33,8:41	./.	./.	./.	0/1:51,15:66	./.
Dock3	chr9:106929944	TCA	T	c.4107+74_4107+75delTG		intron_variant(MODIFIER)	ENSMUST00000044532	rs256120015	0/1:25,13:45	0/1:8,7:18	0/1:7,7:16	./.	./.	0/1:23,9:38	./.	0/1:29,14:45
Mlh1	chr9:111253013	CA	C	n.694+2614delT		intron_variant(MODIFIER)	ENSMUST00000135218	.	0/1:59,25:110	0/1:39,19:74	./.	./.	./.	0/1:30,20:65	./.	0/1:0,7:141
Ctnnb1	chr9:120950606	C	A	c.98C>A	p.Ser33Tyr	missense_variant(MODERATE|MSSEN		.	./.	./.	./.	./.	./.	0/1:23,5:28	./.	./.
Ctnnb1	chr9:120950630	C	T	c.122C>T	p.Thr41Ile	missense_variant(MODERATE|MSSEN	ENSMUST00000145093	.	./.	./.	0/1:23,14:37	0/1:12,6:18	./.	./.	./.	./.
Ctnnb1	chr9:120950642	C	T	c.134C>T	p.Ser45Phe	missense_variant(MODERATE|MSSEN		.	./.	./.	./.	./.	./.	./.	./.	0/1:11,6:17

The clinical significance of particular SNV was determined by searching several databases. After annotation we checked UniProt[19] for functional consequences of an amino acid change. Additionally, we performed a protein BLAST to identify the homologous protein and position of the functional change in humans to check the clinical association in the COSMIC database [20].

Table S9. Classification of functional consequences of detected amino acid changes.

Gene	Chr:Pos	REF	ALT	Codon variant	Functional Variant	Functional Consequence	UniProt	BLAST human (homolog position)	COSMIC Annotation
Apc	chr18:34312747	C	T	c.2695C>T	p.Gln899*	stop_gained(HIGH|NONSENSE)	-	Q901*	Pathogenic (score 0.91)
Apc	chr18:34316309	A	G	c.6257A>G	p.Asp2086Gly	missense_variant(MODERATE)	no functional significance	D2087G	not annotated
Fbxw7	chr3:84903756	A	G	c.187A>G	p.Asn63Asp	missense_variant(MODERATE|MISSENSE)	no functional significance	without homology at this position	not annotated
Fbxw7	chr3:84903911	A	G	c.342A>G	p.Glu114Glu	synonymous_variant(LOW|SILENT)	no functional significance	E114E	not annotated
Fbxw7	chr3:84954904	A	G	c.540A>G	p.Glu180Glu	synonymous_variant(LOW|SILENT)	no functional significance	E180E	not annotated
Pole	chr5:110299343	A	C	c.2081A>C	p.Lys694Thr	missense_variant(MODERATE|MISSENSE)	no record	K694T	not annotated
Arid1a	chr4:133689170	ATATAC	A	c.3289_3293delTATAC	p.Gln1096fs	synonymous_variant(LOW|SILENT)	no record	Q1096fs	not annotated
Ctnnb1	chr9:120950606	C	A	c.98C>A	p.Ser33Tyr	missense_variant(MODERATE|MISSENSE)	target for HIPK2 phosphorylation/ proteasomal degradation	S33Y	Pathogenic (score 0.97)
Ctnnb1	chr9:120950630	C	T	c.122C>T	p.Thr41Ile	missense_variant(MODERATE|MISSENSE)	target for GSK3 phosphorylation	T41I	Pathogenic (score 0.98)
Ctnnb1	chr9:120950642	C	T	c.134C>T	p.Ser45Phe	missense_variant(MODERATE|MISSENSE)	target for secondary GSK3 phosphorylation	S45F	Pathogenic (score 0.98)

Single molecule FISH (smFISH)

Mice were sacrificed and the small intestine was removed and flushed with cold PBS. Small intestine tissue was opened longitudinally and spread on whatman filter paper. Flat tissue was then fixed in 4% paraformaldehyde (PFA, Santa Cruz Biotechnology, sc-281692) in PBS for 3 hours and subsequently incubated in a 30% sucrose, 4% PFA in PBS solution at 4°C overnight with gentle agitation. Fixed tissues were then embedded in Tissue-Tek OCT Compund (Sakura, 4583) and stored at -80°C. 7μm thick sections of fixed tissue were sectioned onto poly L-lysine coated coverslips and used for smFISH staining. Probe libraries were designed using the Stellaris FISH Probe Design Software (Biosearch Technologies), see Tables S10-S12 for complete list of smFISH probes. Probe libraries were coupled to Cy5 (*Mcl1*) or Alexa594 (*Atoh1* or *Wnt2b*). Tissue sections were hybridized with smFISH probe sets based on a previously published protocol[21]. smFISH imaging was performed on a Leica THUNDER Imager 3D Cell Imaging system using the following THUNDER Computational Clearing Settings, Feature Scale (nm): 383, Strength (%): 97.75, Deconvolution settings: Auto and Optimization: High. Objective: 100X/1.4. Quantification of smFISH was performed as previously described using the TransQuant software[22]. Atoh1 smFISH quantification was performed by selecting 7 *Mcl1* expressing and 7 *Mcl1* deficient crypts from the small intestines of 3 different $Mcl1^{\Delta IEC}$ mice. Individual epithelial cells were identified within each crypt and quantification was performed by determining the amount of single RNA molecules per epithelial cell.

Table S10. *Mcl1* probes for smFISH

Mcl1	
mus_*Mcl1*_1	caggccaaacatggtcggac
mus_*Mcl1*_2	tacaggttcaagccgatgac
mus_*Mcl1*_3	caagtagcgcgagatgatct
mus_*Mcl1*_4	atcgccttcgttttaatgt
mus_*Mcl1*_5	agtttgttacgccatctttg
mus_*Mcl1*_6	attgcactcacaaggctatc
mus_*Mcl1*_7	tggctggagctttaagagtc
mus_*Mcl1*_8	cacatgttttcacagatgca
mus_*Mcl1*_9	cagacagtgactcttccagg
mus_*Mcl1*_10	cactctgagcagagtaatgg
mus_*Mcl1*_11	ttctagtcatcgtttggtga
mus_*Mcl1*_12	acagggctaaaagtcctgag
mus_*Mcl1*_13	tcaagtacttttggccatc
mus_*Mcl1*_14	aatcgaggctgttcagtttt
mus_*Mcl1*_15	aggctctgcatatacactag
mus_*Mcl1*_16	ccctgcatagttataaatct
mus_*Mcl1*_17	tcttacatctatctacctgt
mus_*Mcl1*_18	tgtaagtcaacaggggatca
mus_*Mcl1*_19	taagactctagcctgcttta
mus_*Mcl1*_20	taaacccagtgaatagcacc
mus_*Mcl1*_21	caccaggtataaacttgtgt
mus_*Mcl1*_22	cttggcaatccttagtagac
mus_*Mcl1*_23	acgccaacagtaaaggaagt
mus_*Mcl1*_24	ataggggaactgggagcata
mus_*Mcl1*_25	gggaggaagtgtagacgact
mus_*Mcl1*_26	aaaatggccagtgaagagca
mus_*Mcl1*_27	ggctcaaagagcaagtgttc
mus_*Mcl1*_28	gtaacaatggaaagcatgcc
mus_*Mcl1*_29	ggacctttgatgtttttctt
mus_*Mcl1*_30	ccaacctttgaaattcccaa
mus_*Mcl1*_31	acacagtcatacttggagca
mus_*Mcl1*_32	tttgttaaccgagtttagca
mus_*Mcl1*_33	aataccttcagttaccagtg
mus_*Mcl1*_34	gattcctgcctatttttatc
mus_*Mcl1*_35	acttcttccctattacattc
mus_*Mcl1*_36	caggtacaaatcactcccaa
mus_*Mcl1*_37	aagtgctctgaagtccgaag
mus_*Mcl1*_38	agaggctaacctttagtca
mus_*Mcl1*_39	gaagtcaggctcctagtaaa
mus_*Mcl1*_40	ttcatttcacccttgtgag
mus_*Mcl1*_41	ccctggacctaaaataccta
mus_*Mcl1*_42	catctagtcagcactcagac
mus_*Mcl1*_43	gatgcttgaagactgcatgt
mus_*Mcl1*_44	tgttcacccagatagaatgt
mus_*Mcl1*_45	aggtgctctaccagaatgaa
mus_*Mcl1*_46	ctttcgggaacagctgttaa
mus_*Mcl1*_47	taacttgcagttggtcctaa
mus_*Mcl1*_48	aggggaacatttacaaccca

Table S11. *Atoh1* probes for smFISH

Atoh1	
mus_*Atoh1*_1	gatttttttccttcctcct
mus_*Atoh1*_2	ttcctagtctcttctgcaag
mus_*Atoh1*_3	cccgaacaacaacaacaaaa
mus_*Atoh1*_4	cagttcaacgaaggggataa
mus_*Atoh1*_5	ttttacctcagcccactctt
mus_*Atoh1*_6	tatccaggagggacagttct
mus_*Atoh1*_7	tgcaaagtgggagtcagcca
mus_*Atoh1*_8	agaatgcagcagatactggg
mus_*Atoh1*_9	tctccttaccagctcaccct
mus_*Atoh1*_10	agctgttcccgtactttgac
mus_*Atoh1*_11	acaaccccacccttcagctt
mus_*Atoh1*_12	attcacctgtttgctggaag
mus_*Atoh1*_13	agcctcctttgcttctgtac
mus_*Atoh1*_14	ttgaaggacgggataacgtt
mus_*Atoh1*_15	tttggacagcttcttgtcgt
mus_*Atoh1*_16	ttgatgtagatctgggccat
mus_*Atoh1*_17	attgggagtctgcagcaact
mus_*Atoh1*_18	atttttgcaggaagctgtgg
mus_*Atoh1*_19	tgtgccatcatcgctgttag
mus_*Atoh1*_20	tttgctgttgtcctcctgta
mus_*Atoh1*_21	ttctgtgggatctgggagat
mus_*Atoh1*_22	taatgagagtgggggggaaaa
mus_*Atoh1*_23	aactggcctcatcagagtca
mus_*Atoh1*_24	tttcagggagctgttgcctt
mus_*Atoh1*_25	aagggcatttggttgtctca
mus_*Atoh1*_26	aagggtgcagggatatttgt
mus_*Atoh1*_27	cgatcaccacagaccaaaaa
mus_*Atoh1*_28	gaagtcaagtcgttgctaac
mus_*Atoh1*_29	taggaggaaggggattggaa
mus_*Atoh1*_30	ctacatacagaggaaggaga
mus_*Atoh1*_31	gatgccacgtaaaggtacat
mus_*Atoh1*_32	atattggcagcatggaccat
mus_*Atoh1*_33	cagagatacgacattttagc
mus_*Atoh1*_34	taagtgaaacccagaccaga
mus_*Atoh1*_35	ggatgaactcccaaggtata
mus_*Atoh1*_36	atttgtgagtgagcgcaaca
mus_*Atoh1*_37	ggggaaacaacttcattgac
mus_*Atoh1*_38	aaagtacccaatgcgggtct
mus_*Atoh1*_39	caacacaatagtccgtgttc
mus_*Atoh1*_40	cttatctgcccctgcatttt
mus_*Atoh1*_41	ggtgtctaagctctacagat
mus_*Atoh1*_42	tagacacactgctggacaca
mus_*Atoh1*_43	atgaagtgcgtgtattctgg
mus_*Atoh1*_44	ttgagtttcttcaaggcggc
mus_*Atoh1*_45	aaaagttgctctgcattggc
mus_*Atoh1*_46	ccaaatgcctttgacactac
mus_*Atoh1*_47	gaaatgggtccaaatacgca
mus_*Atoh1*_48	cgatctcgagtagaaaatgt

Table S12. *Wnt2b* probes for smFISH

Wnt2b	
mus_*Wnt2b*_1	ggatgttgtcacagatcact
mus_*Wnt2b*_2	tactgagcgcatgatgtctg
mus_*Wnt2b*_3	atagcatagacgaacgctgc
mus_*Wnt2b*_4	atggatgttgtcactacagc
mus_*Wnt2b*_5	ttgtgtaagttcatgagggc
mus_*Wnt2b*_6	agtagacaagatcagtccgg
mus_*Wnt2b*_7	tagaagtcttgctgcagacg
mus_*Wnt2b*_8	aacacatgatttcacaccca
mus_*Wnt2b*_9	gtggaatttgcactcacact
mus_*Wnt2b*_10	atgtgtggacatccacagtg
mus_*Wnt2b*_11	ttgtgcttttgagtcagagg
mus_*Wnt2b*_12	ggattgagggtagaggaagg
mus_*Wnt2b*_13	cgtgacagaagccatagcag
mus_*Wnt2b*_14	taaatccatcccctatcaac
mus_*Wnt2b*_15	ccttgacttagtgcaactca
mus_*Wnt2b*_16	tgcaagcaaaggggaggatg
mus_*Wnt2b*_17	gcatacccaaagaggatcag
mus_*Wnt2b*_18	tcaaacacggaagctacctc
mus_*Wnt2b*_19	gacaggcagttttatctctg
mus_*Wnt2b*_20	actatggcctaagattgtct
mus_*Wnt2b*_21	taacccatctagctatctca
mus_*Wnt2b*_22	atgtggagccttgttcaatg
mus_*Wnt2b*_23	ccactactttataagctgcg
mus_*Wnt2b*_24	agagcattgtgattttcctc
mus_*Wnt2b*_25	ggcacagagaatgtgtatct
mus_*Wnt2b*_26	gtaagaatttgacccactgc
mus_*Wnt2b*_27	attctctcacaatcctgttc
mus_*Wnt2b*_28	cgaatctccggaatagtgga
mus_*Wnt2b*_29	gctgaagatcctcaagaact
mus_*Wnt2b*_30	aaggccttataggatgtttg
mus_*Wnt2b*_31	tagttaacagttggacctgg
mus_*Wnt2b*_32	ctgtttaagtcgatcgtgga
mus_*Wnt2b*_33	cagtagcacagagagaacct
mus_*Wnt2b*_34	ctagaccatcaaggtttgga
mus_*Wnt2b*_35	aagatgaccattgtcgaggt
mus_*Wnt2b*_36	tgatgacgtctatcagtcgg
mus_*Wnt2b*_37	acagccctaaatcagaaggt
mus_*Wnt2b*_38	gaatctagtctgttgtctgc
mus_*Wnt2b*_39	agaattccttgtgaaagcct
mus_*Wnt2b*_40	tgctccacaaacatctgaga
mus_*Wnt2b*_41	caaatcccctcaccaaaaga
mus_*Wnt2b*_42	gactagctcatgttttgtgt
mus_*Wnt2b*_43	ctactctgcgaggaagacat
mus_*Wnt2b*_44	aaactcctctcttccaagag
mus_*Wnt2b*_45	accgtaacttggatgttctc
mus_*Wnt2b*_46	aagtagatttacctcaggct
mus_*Wnt2b*_47	gagatgtcacagatgtctgc
mus_*Wnt2b*_48	atcagctagaatttggagcc

RNASeq

For RNASeq analysis, RNA was extracted from small intestinal tissue that had been frozen in RNAlater (Sigma-Aldrich); taken from mice sacrificed 3 or 4 days post induction. RNA extraction and DNA digestion was performed on homogenised tissue using QIAGEN RNeasy Mini Kit (QIAGEN, #74104) according to the manufacturer's instructions. The quality of the purified RNA was tested on an Agilent 2200 Tapestation using RNA screentape. Libraries for cluster generation and RNA sequencing were prepared following an adapted method from Fisher *et al*., 2011 [23] using an Illumina TruSeq RNA LT Kit v2. Libraries were run on the Illumina NextSeq 500 using the High Output 75 cycles kit (2x36cycles, paired end reads, single index) [24]. Quality control of the raw RNASeq data files was performed by fastqc (http://www.bioinformatics.babraham.ac.uk/projects/fastqc/) and fastq_screen (http://www.bioinformatics.babraham.ac.uk/projects/fastq_screen/). Next, RNASeq reads were aligned to the mouse genome (GRCm38.75) using TopHat2 (tophat2), and gene level counts were determined from the resulting bam files using htseq_count (http://www-huber.embl.de/users/anders/HTSeq/doc/count.html) with default settings. Differential expression analysis and data normalisation was performed using the R package DESeq2, with statistically significant differences in gene expression defined using a false discovery rate (FDR) of 5% or 10%. A detailed list of signaling pathways enriched in i-*Mcl*1$^{\Delta IEC}$ mice compared with wild type control mice is shown in Table S13. A table of linked toxic pathologies associated with up-regulated genes detected in i-*Mcl1*$^{\Delta IEC}$ mice are listed in Table S14.

GSEA analysis was performed using the GSEA v2.0 software (Broad Institute). The reference gene sets were obtained from published sources as follows; genes upregulated following APC loss [25] & WNT target genes commonly upregulated in human colorectal cancer [26].

841 **Table S13**. Pathways enriched in i-*Mcl1*$^{\Delta IEC}$ mice compared with wild type control mice.

#	Pathways Enriched in i-Mcl-1$^{\Delta IEC}$ mouse small intestine	p-value	FDR
1	Cell cycle_Start of DNA replication in early S phase	1.249E-10	1.123E-07
2	Cell cycle_Nucleocytoplasmic transport of CDK/Cyclins	2.142E-07	8.790E-05
3	Apoptosis and survival_Role of IAP-proteins in apoptosis	3.307E-07	8.790E-05
4	Cell cycle_Regulation of G1/S transition (part 1)	4.557E-07	8.790E-05
5	Cell cycle_Role of SCF complex in cell cycle regulation	6.619E-07	8.790E-05
6	CAR signaling via cross-talk / Human Version	6.844E-07	8.790E-05
7	Cell cycle_Regulation of G1/S transition (part 2)	6.844E-07	8.790E-05
8	CAR signaling via cross-talk / Rodent version	1.325E-06	1.489E-04
9	Regulation of metabolism_Bile acids regulation of glucose and lipid metabolism via FXR	1.535E-06	1.533E-04
10	Development_Regulation of telomere length and cellular immortalization	3.090E-06	2.558E-04
11	Transcription_Epigenetic regulation of gene expression	3.345E-06	2.558E-04
12	Cytoskeleton remodeling_TGF, WNT and cytoskeletal remodeling	3.414E-06	2.558E-04
13	Development_EGFR signaling pathway	6.640E-06	4.592E-04
14	ATP/ITP metabolism	8.389E-06	5.387E-04
15	Cell cycle_Cell cycle (generic schema)	1.064E-05	6.375E-04
16	GTP-XTP metabolism	1.195E-05	6.581E-04
17	Development_WNT signaling pathway. Part 2	1.244E-05	6.581E-04
18	Development_Prolactin receptor signaling	1.767E-05	8.827E-04
19	Cell cycle_ESR1 regulation of G1/S transition	3.214E-05	1.521E-03
20	Transcription_Ligand-dependent activation of the ESR1/SP pathway	4.102E-05	1.844E-03

842

843

844

845

846

847

848

849

850

851

852 **Table S14**. Toxic pathologies associated with genes enriched in i-*Mcl1*$^{\Delta IEC}$ mice compared with

853 wild type control mice.

#	Toxic pathologies in i-Mcl-1$^{\Delta IEC}$ mouse small intestine	p-value	FDR
1	Small intestine, intestinal epithelium injury	7.194E-09	1.743E-05
2	Small intestine, mucosa-degeneration	6.027E-08	5.141E-05
3	Jejunum, mucosa-degeneration	6.473E-08	5.141E-05
4	Jejunum-degeneration	1.156E-07	5.141E-05
5	Jejunum, mucosa, intestinal epithelium injury	1.252E-07	5.141E-05
6	Small intestine-degeneration	1.352E-07	5.141E-05
7	Intestinal epithelium injury	1.489E-07	5.141E-05
8	Intestine-regeneration	1.697E-07	5.141E-05
9	Intestine-degeneration	2.613E-07	7.034E-05
10	Small intestine, mucosa injury	3.871E-07	9.380E-05
11	Liver-centrilobular regeneration	5.995E-07	1.321E-04
12	Jejunum, mucosa injury	9.324E-07	1.883E-04
13	Jejunum injury	1.852E-06	3.045E-04
14	Large intestine-regeneration	1.885E-06	3.045E-04
15	Colon-regeneration	1.885E-06	3.045E-04
16	Small intestine, mucosa-apoptosis	2.907E-06	4.402E-04
17	Colon, mucosa-regeneration	3.785E-06	5.095E-04
18	Large intestine, mucosa-regeneration	3.785E-06	5.095E-04
19	Small intestine injury	4.707E-06	6.003E-04
20	Small intestine-apoptosis	5.326E-06	6.391E-04

854

855

856

857

858

859

860

861

862

Supplemental References

1. Smith K, McCoy KD, Macpherson AJ. Use of axenic animals in studying the adaptation of mammals to their commensal intestinal microbiota. Semin Immunol 2007;19:59-69.
2. Vick B, Weber A, Urbanik T, et al. Knockout of myeloid cell leukemia-1 induces liver damage and increases apoptosis susceptibility of murine hepatocytes. Hepatology 2009;49:627-36.
3. Weber A, Boger R, Vick B, et al. Hepatocyte-specific deletion of the antiapoptotic protein myeloid cell leukemia-1 triggers proliferation and hepatocarcinogenesis in mice. Hepatology 2010;51:1226-36.
4. el Marjou F, Janssen KP, Chang BH, et al. Tissue-specific and inducible Cre-mediated recombination in the gut epithelium. Genesis 2004;39:186-93.
5. Opferman JT, Letai A, Beard C, et al. Development and maintenance of B and T lymphocytes requires antiapoptotic MCL-1. Nature 2003;426:671-6.
6. Brault V, Moore R, Kutsch S, et al. Inactivation of the beta-catenin gene by Wnt1-Cre-mediated deletion results in dramatic brain malformation and failure of craniofacial development. Development 2001;128:1253-64.
7. Shibata H, Toyama K, Shioya H, et al. Rapid colorectal adenoma formation initiated by conditional targeting of the Apc gene. Science 1997;278:120-3.
8. Propheter DC, Chara AL, Harris TA, et al. Resistin-like molecule beta is a bactericidal protein that promotes spatial segregation of the microbiota and the colonic epithelium. Proc Natl Acad Sci U S A 2017;114:11027-11033.
9. Packey CD, Shanahan MT, Manick S, et al. Molecular detection of bacterial contamination in gnotobiotic rodent units. Gut Microbes 2013;4:361-70.
10. Erben U, Loddenkemper C, Doerfel K, et al. A guide to histomorphological evaluation of intestinal inflammation in mouse models. Int J Clin Exp Pathol 2014;7:4557-76.
11. Boivin GP, Washington K, Yang K, et al. Pathology of mouse models of intestinal cancer: consensus report and recommendations. Gastroenterology 2003;124:762-77.
12. Huang H, Ushijima T, Nagao M, et al. Beta-catenin mutations in liver tumors induced by 2-amino-3,4-dimethylimidazo[4,5-f]quinoline in CDF1 mice. Cancer Lett 2003;198:29-35.
13. Wolf MJ, Adili A, Piotrowitz K, et al. Metabolic activation of intrahepatic CD8+ T cells and NKT cells causes nonalcoholic steatohepatitis and liver cancer via cross-talk with hepatocytes. Cancer Cell 2014;26:549-64.
14. Fred T. Bosman FC, Ralph H. Hruban, Neil D. Theise. Tumours of the colon and rectum. WHO Classification of Tumours of the Digestive System. Volume 4th Edition: WHO Press, 2010:140-142.
15. Li H, Durbin R. Fast and accurate short read alignment with Burrows-Wheeler transform. Bioinformatics 2009;25:1754-60.
16. DePristo MA, Banks E, Poplin R, et al. A framework for variation discovery and genotyping using next-generation DNA sequencing data. Nat Genet 2011;43:491-8.
17. Cingolani P, Platts A, Wang le L, et al. A program for annotating and predicting the effects of single nucleotide polymorphisms, SnpEff: SNPs in the genome of Drosophila melanogaster strain w1118; iso-2; iso-3. Fly (Austin) 2012;6:80-92.
18. Fairfield H, Srivastava A, Ananda G, et al. Exome sequencing reveals pathogenic mutations in 91 strains of mice with Mendelian disorders. Genome Res 2015;25:948-57.
19. UniProt: a hub for protein information. Nucleic Acids Res 2015;43:D204-12.
20. Forbes SA, Beare D, Gunasekaran P, et al. COSMIC: exploring the world's knowledge of somatic mutations in human cancer. Nucleic Acids Res 2015;43:D805-11.
21. Moor AE, Harnik Y, Ben-Moshe S, et al. Spatial Reconstruction of Single Enterocytes Uncovers Broad Zonation along the Intestinal Villus Axis. Cell 2018;175:1156-1167.e15.
22. Bahar Halpern K, Itzkovitz S. Single molecule approaches for quantifying transcription and degradation rates in intact mammalian tissues. Methods 2016;98:134-142.
23. Fisher S, Barry A, Abreu J, et al. A scalable, fully automated process for construction of sequence-ready human exome targeted capture libraries. Genome Biol 2011;12:R1.
24. Rath N, Morton JP, Julian L, et al. ROCK signaling promotes collagen remodeling to facilitate invasive pancreatic ductal adenocarcinoma tumor cell growth. EMBO Mol Med 2017;9:198-218.
25. Sansom OJ, Reed KR, Hayes AJ, et al. Loss of Apc in vivo immediately perturbs Wnt signaling, differentiation, and migration. Genes Dev 2004;18:1385-90.
26. Van der Flier LG, Sabates-Bellver J, Oving I, et al. The Intestinal Wnt/TCF Signature. Gastroenterology 2007;132:628-32.